

國立臺灣大學理學院地理環境資源學系

博士論文

Department of Geography

College of Science

National Taiwan University

Doctoral Dissertation



亞熱帶亞高山矮竹地上部碳儲存量空間變異  
及影響因子

Subtropical dwarf bamboo aboveground carbon storage  
spatial variation and influencing factors in subalpine  
Taiwan

潘孝隆

Hsiao-Lung Pan

指導教授：黃倬英 博士

Advisor: Cho-ying Huang, PhD.

中華民國 112 年 7 月

July 2023



國立臺灣大學博士學位論文  
口試委員會審定書

PHD DISSERTATION ACCEPTANCE CERTIFICATE  
NATIONAL TAIWAN UNIVERSITY

亞熱帶亞高山矮竹地上部碳儲存量空間變異及影響因子

Subtropical dwarf bamboo aboveground carbon storage  
spatial variation and influencing factors in subalpine  
Taiwan

本論文係潘孝隆(學號 D07228003) 在國立臺灣大學地理環境資源學系完成之博士學位論文，於民國 112 年 7 月 14 日承下列考試委員審查通過及口試及格，特此證明。

The undersigned, appointed by the Department of Geography on 14 July 2023 have examined a PhD dissertation entitled above presented by Hsiao-Lung Pan (D07228003) candidate and hereby certify that it is worthy of acceptance.

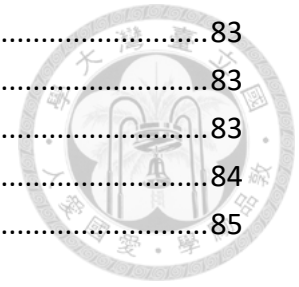
口試委員 Oral examination committee:

<u>黃偉英</u> (指導教授 Advisor)	<u>莊子敬</u>	_____
<u>林政道</u>	<u>張在弘</u>	_____
<u>鍾智昕</u>		_____
系主任/所長 Director: <u>黃志川</u>		_____

## Table of Content

論文口試委員會審定書.....	i
謝辭.....	iv
中文摘要.....	v
ABSTRACT.....	vi
INTRODUCTION .....	1
I. Alpine and subalpine bamboo influence on vegetation range shift .....	1
II. Expansion of dwarf bamboo ( <i>Yushania niitakayamensis</i> ).....	2
III. Application of UAV-lidar on AGB or AGC density .....	3
IV. Dissertation overview.....	5
PRESENT STUDY .....	6
I. Summary.....	6
II. Future work .....	10
III. Conclusions.....	14
REFERENCES .....	16
APPENDIX A. Mapping aboveground carbon density of subtropical subalpine dwarf bamboo ( <i>Yushania niitakayamensis</i> ) vegetation using UAV-lidar .....	22
Abstract .....	23
1. Introduction.....	24
2. Materials and Methods.....	25
3. Results.....	37
4. Discussion .....	45
5. Conclusions.....	49
Acknowledgments.....	49
Declaration of interest statement .....	50
Author contributions statement.....	50
Data availability statement.....	50
Declaration of Generative AI and AI-assisted technologies in the writing process .....	50
References.....	51
APPENDIX B. Spatial clustering moderates the subalpine dwarf bamboo AGC density on environmental gradients in a tropical island.....	58
Abstract .....	59
1. Introduction.....	61
2. Materials and methods .....	63
3. Results.....	72
4. Discussions .....	78
5. Conclusion .....	82

Acknowledgments.....	83
Declaration of interest statement .....	83
Author contributions statement.....	83
Data availability statement.....	84
References.....	85



## 謝 辭

玉山箭竹能生長在海拔一千多公尺，一路延伸到寒冷乾燥的三千多公尺；在開闊地的體型雖是十幾公分的毯狀植被，但森林下層則是疏密不均、高度3-4公尺的竹桿。密生箭竹會阻礙高海拔冠層的樹種(如冷杉)小苗生長，而在中高海拔人工林地，則常入侵栽植地點；它既利用地下莖繁殖，拓展生長範圍，火燒或干擾後，能萌發新桿，迅速覆蓋；也利用穎果傳播，雖然開花、結果是長週期事件，但伴隨開花後的小面積枯死與潛在負面生態影響亦頗受重視。

當暖化已成進行式，大量學術研究報導低海拔的植物向上拓殖，進而稀釋高海拔植物物種多樣性的趨勢。我好奇，似玉山箭竹如此優勢(侵略性高)的物種是否更為優勢，抑或自身配合暖化的環境，調整外型與生理，變得更相對優勢或過度優勢，而影響較低海拔植物向高海拔擴張。另一方面，因玉山箭竹為輕質燃料，暖化下的優勢可能增強燃料的水平與垂直連續性以及燃料量，一旦野火發生，則必然涉及高山活動安全、避難疏散、碳儲量管理、以及其他物種棲地等議題；然而，此提問需要多個研究子題支撐，而細尺度、地景層級的估測與空間分布即為根本子題。博士班階段，我聚焦於以無人機光達的測繪技術估計地上部碳儲存量(可轉換為地上部生物量、燃料量)，進而探索空間變異與環境、生物因子間的關係，先著重細尺度的測計並檢驗假說，期盼未來能接續其他子題的研究。

我想感謝指導教授黃倬英老師，支持我構思研究提問。老師對於研究議題重要性的敏銳，讓我更聚焦於研究的基礎與推展階段，也同時指出研究的弱點，助我省去旁枝末節與嘗試錯誤可能虛擲的時間，進而定心投入精力與時間。也特別感謝口試委員們提供寶貴建議及疑問，促使我從不同角度解讀與反思研究的結果與可能的謬誤，並據以修正論文。

藉此機會，我想謝謝羅東聖母醫院李惟陽學長、臺師大廖學誠老師、時任羅東林區管理處的陳新旗主任，三人的激勵與鼓舞，讓我在林區管理處及工作站磨練11年後，決心回到研究領域，重拾夢想。謝謝老同學仕偉，在我緊急就醫時，奔走與諸多協助，我才有機會回台北工作，完成未竟的夢想。

我也想謝謝在第一次讀博士班時，江金倉老師與趙蓮菊老師的解惑與鼓勵；在碩士與大學期間，陳昭明老師、林文亮老師、邱祈榮老師與林朝欽博士的引導與點撥；也謝謝普訊融悟文教基金會的獎助，讓我有更多時間專注於學習、思考與野外工作。我也要感恩蔣夫人、華興育幼院暨華興中學，謝謝蔡照平老師、鄭輝源老師、許維忠老師、沈素燕老師與李月娟教官的關心與教導。

感謝農業委員會(農業部)林業試驗所提供進修機會，曾彥學所長的鼓勵、技術服務組劉一新前組長、胡元璋組長的支持與協助，讓我在公務之餘，有精神與體力完成學業，也感謝紬君、心瑀、涵縈、雅惠、子瑩細心協助整理箭竹樣本。最後，感謝所有家人的支持，我才能專注完成博士班的各個重要階段；感恩許多師長、同學、同事與許多在士農工商努力的朋友們協助。我得之於人者太多，謝謝引路人默默指引與提醒。謝 天、謝 地。

## 中文摘要



高山和亞高山地區，矮竹優勢與氣候變遷引起的植被組成改變間的互動極具意義。本論文深入探討矮竹的優勢及碳儲存空間變化的生態意義，內容包含兩個主要研究的關鍵成果。

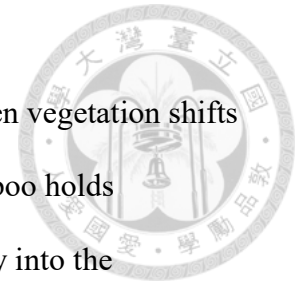
第一個研究為首次將無人機光達技術(UAV-lidar)與線性模型結合並應用於矮竹，以準確估算矮竹植被中的地上碳儲存(AGC)密度。其中，多變量自適應迴歸樣條(MARS)在AGC密度估算中優於其他模式類型，其測試資料集RMSE為 $0.15 \text{ (kgC m}^{-2}\text{)}$ 且殘差全距最短，因此所估計的AGC密度圖可應用於管理與相關研究。MARS模式亦顯示近冠層底部高度為關鍵變數，有別於傳統僅關注冠層頂部高度的模式型態，另估計出的AGC密度圖顯示出顯著空間變異，並可能與坡度陡峭程度有關。

第二個研究深入瞭解AGC密度與生物及非生物因子間關係，變數包括空間聚集類型、太陽輻射、風和微地形等影響亞高山植被的重要因子。分析結果顯示，空間聚集類型顯著影響AGC密度對環境變數的反應。空間聚集增強環境因子對AGC密度的影響。儘管空間聚集類型內的冷區不受環境因子影響，但熱區對輻射、風型和微地形的變化則呈現出不同的反應，因相同的環境因子卻呈現反差的反應，顯示矮竹AGC密度對這些條件的馴化情形。

本論文將植被AGC密度與環境因子相互關係緊密結合，提供持續暖化的氣候情境中優化保育和管理策略的重要資訊。

關鍵字:矮竹、無人機光達、地上部碳儲存密度、多變量自適應迴歸樣條、空間群聚、氣候適應

## ABSTRACT



In the alpine and subalpine regions, the intricate interplay between vegetation shifts driven by climate change and the dominant presence of dwarf bamboo holds paramount significance. This comprehensive research delves deeply into the ecological implications of dwarf bamboo's prevalence and carbon storage dynamics. This dissertation encapsulates the pivotal outcomes of two primary studies.

The initial study pioneers the integration of UAV-lidar technology and linear models. This synergy accurately estimates aboveground carbon (AGC) density in dwarf bamboo vegetation. Notably, multivariate adaptive regression splines (MARS) outperform other models in AGC density estimation, with a root mean square error (RMSE) of 0.15 (kgC m<sup>-2</sup>) on test data and the shortest residual range. The model identified near-canopy bottom height as a crucial predictor, challenging the conventional focus on canopy top height. The estimated AGC density map unveiled substantial spatial variation, which may link to slope steepness.

On the other hand, the intricate relationship between AGC density and various factors comes under scrutiny in the second study. These include spatial clustering, solar irradiation, wind patterns, and microtopography. Spatial clustering significantly shapes how AGC density responds to environmental variables. The role of spatial clustering is pivotal, intensifying the effect of environmental conditions on AGC density. While coldspots remain unresponsive, hotspots exhibit distinct reactions to changes in irradiation, wind patterns, and microtopography. This variation in response to shared environmental factors suggests acclimation to these conditions.

This research piece weaves together a comprehensive understanding of the

interplay between vegetation AGC density and environmental forces. It provides essential information for refining conservation and management strategies amidst evolving climatic scenarios.



Keywords: dwarf bamboo, AGC density, UAV-lidar, MARS, spatial clustering, climate adaptation.



# INTRODUCTION

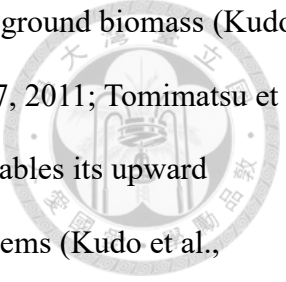
## I. Alpine and subalpine bamboo influence on vegetation range shift

Climate change and alterations in water availability are driving shifts in terrestrial vegetation distribution and diversity (Higgins et al., 2023; Pauli et al., 2012). Among the vegetation types extending their range to higher latitudes and elevations, bamboo stands out as an efficient carbon sink and provider of key ecosystem services such as food, construction materials, and soil erosion regulation (Yuen et al., 2017). However, the potential invasive tendencies of bamboo raise concerns about their impact on plant biodiversity (Xu et al., 2020; Bai et al., 2016; Canavan et al., 2016).

Bamboos are widespread along forest edges, forming large patches or growing beneath canopies in regions across South Asia, East Asia, Africa, and Central and South America (Guerreiro, 2014; Kudo et al., 2011; van der Hoek et al., 2019; Ye et al., 2019). Their clonal propagation strategy, categorized as clumping or running growth, shapes their distribution patterns. Clumping bamboo generates new shoots from a central clump, while running bamboo extends rhizomes to produce new culm shoots, contributing to its potential for invasive expansion (Xu et al., 2020; Takano et al., 2017).

Bamboo significantly influences light availability, soil moisture, and herbivory, which, in turn, affects the survival of tree seedlings. This ecological filtering process impacts the composition and diversity of local floristic communities (Bona et al., 2020; Caccia et al., 2009; Kudo et al., 2017; Larpkern et al., 2011).

Dwarf bamboo is a group of small-sized bamboo species found expanding up to or gaining dominance/overdominance in subalpine and alpine areas (Kudo et al., 2011; Winkler et al., 2016). The expansion of dwarf bamboo in subalpine and alpine regions



raises concerns about its influence on local plant diversity and aboveground biomass (Kudo et al., 2011; Winkler et al., 2016; Gaira et al., 2022; Kudo et al., 2017, 2011; Tomimatsu et al., 2011). Meanwhile, the phenotypic plasticity of dwarf bamboo enables its upward migration and amplifies its impact on local communities and ecosystems (Kudo et al., 2018). Dwarf bamboo also functions as an ecological filter in montane, subalpine, and alpine areas, affecting abundance and diversity (Itô & Hino, 2007; Kudo et al., 2017; Hirobe et al., 2015). Additionally, aboveground biomass (AGB) of dwarf bamboo has adverse relationships with the seedlings' survival rate of major tree species, while some are affected more profoundly than others (Itô & Hino, 2007). AGB is part of biomass, a measure of plant fitness to the environment, and aggregately a response of an ecosystem to climate change (Younginger et al., 2017). Meanwhile, aboveground carbon storage (AGC) can be converted from AGB with an AGB-carbon conversion coefficient from elemental analysis, and these two values are proportional; therefore, the trend or variation of AGC values also indicates that of AGB values.

However, a significant gap exists in our understanding, as previous studies have often focused on bamboo's cover rather than AGB/AGC to measure dominance. This study addresses this gap by emphasizing the importance of estimating AGC as a comprehensive measure of bamboo's contribution to carbon storage. The complexities of bamboo's spatial structure and phenology-driven spectral variability have posed challenges for accurate AGC estimation using traditional optical remote sensing.

## **II. Expansion of dwarf bamboo (*Yushania niitakayamensis*)**

*Yushania niitakayamensis* (Hayata) Keng f., known as Yushan cane, is a subalpine and alpine dwarf bamboo native to south-central China and the Philippines. This species, distributed across temperate eastern Asia and Malesia in Asia-tropical (POWO, 2023),

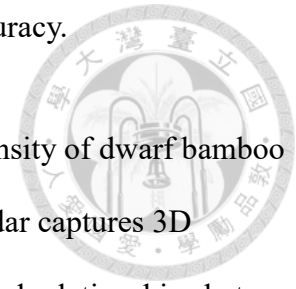
inhabits montane and subalpine environments in Taiwan (Su, 1985). Its growth strategy involves running rhizomes, which produce new culm shoots from the base clump. Distinct short and tall forms characterize *Yushania niitakayamensis*, each with unique attributes driven by environmental factors (Wu & Kao, 2021). This variability contributes to the complex spatial distribution of bamboo and its relationship with neighboring forested areas regarding light conditions. Additionally, environmental factors such as wildfire frequency, aspect, soil moisture, and wind exposure might relate to two body size forms (Chen et al., 1992).

Studies have highlighted the inhibitory effects of dwarf bamboo on natural regeneration and species diversity in forest understories (Liao et al., 2012, 2013) or artificial regeneration (Chang, 1981). The expansion of dwarf bamboo has been reported in alpine areas, impacting biodiversity and ecosystem functioning (Kuo et al., 2021). However, existing literature has primarily focused on bamboo's cover dominance, neglecting key measures such as AGC and AGB, particularly in fine scale, that provide deeper insights into its ecological role or potential management measures. In this study, I proposed hypotheses on the comparative contribution of environmental factors and biotic attributes of acclimation and response of the dwarf bamboo AGB or AGC density on the environmental gradients.

### **III. Application of UAV-lidar on AGB or AGC density**

The estimation of aboveground biomass (AGB) or aboveground carbon (AGC) density using optical remote sensing has been widely applied (Kumar & Mutanga, 2017; Frohling et al., 2009). However, bamboo's intricate canopy structure and phenological variability hinder accurate AGC estimation using spectral features (Cao et al., 2019; Chen et al., 2019). However, lidar (light detection and ranging) technology offers a solution by

leveraging three-dimensional (3D) point cloud data to improve accuracy.



This study utilized lidar point cloud data to estimate the AGC density of dwarf bamboo across complex subalpine terrain. Unlike optical remote sensing, lidar captures 3D structural information, allowing extraction of meaningful metrics and relationships between lidar metrics and AGC density (Beland et al., 2019; Lefsky, Cohen, and Harding et al., 2002; Lefsky, Cohen, and Parker et al., 2002). Airborne lidar data have been extensively used in ecological studies (Matasci et al., 2018; Gregoire et al., 2016; Asner et al., 2009). Lidar point clouds provide valuable insights for modeling canopy height, cover, basal area, biomass, and volume (Roussel et al., 2020).

Unmanned aerial vehicle (UAV) lidar offers a cost-effective alternative to airborne lidar, producing comparable point cloud density (Beland et al., 2019). Its applications include AGB density estimation in various ecosystems, enhancing spatial resolution for inventory, and mapping (Wallace et al., 2012). UAV-lidar data enable inference of fine-scale AGB or AGC, valuable for understanding spatial patterns and variations, especially for non-forest vegetation (da Costa et al., 2021; Madsen et al., 2020; Wang et al., 2017, 2019).

Additionally, UAV-lidar data support the creation of high-resolution digital surface models (DSM) and digital elevation models (DEM), facilitating micro-topographic analysis and downscaled climate element simulations. Combined with fine-scale AGB or AGC density data, these downscaled factors establish AGB/AGC-environment associations. The resulting relationships provide insights into understanding the subalpine ecosystems in a warming future.

#### IV. Dissertation overview

This dissertation research consists of two individual and connected studies to understand the subalpine dwarf bamboo vegetation AGC density spatial variation and related biotic and abiotic factors in fine scale using UAV-lidar point cloud data. I present each study as a separate manuscript in the appendix, and it is submitted and under review or ready for journal submission. I was the main contributor to these works and co-author of these manuscripts, contributing to the editorial, logic, and refinement of the conceptualization. The first research paper (Appendix A) entitled, “Mapping aboveground carbon density of subtropical subalpine dwarf bamboo (*Yushania niitakayamensis*) vegetation using UAV-lidar”, devoted to accurately estimating AGC density in high spatial resolution ( $\text{kgC m}^{-2}$ ) and evaluate the performance of five linear models of dwarf bamboo vegetation in a subalpine area in Central Taiwan, and map the AGC density with multivariate adaptive regression splines (MARS) method. Since AGC can be calculated by the AGB and AGB-carbon conversion coefficient, the trend and spatial variation of AGC density also reflect that of AGB density, which measures the vegetation's fitness. Modeling AGC density, consequently, highlights both the carbon and fitness of the dwarf bamboo. The second research paper (Appendix B), entitled “Spatial clustering moderates the subalpine dwarf bamboo AGC density on environmental gradients in a tropical island,” hypothesized that vegetation spatial clustering conditions the influence of environmental factors on AGC density, which emphasized the canopy structure of the dwarf bamboo, contribute more to AGC density than abiotic factors when the dwarf bamboo is dominant species in the landscape, comparing to conventional emphasis on the influence of abiotic factors.

## PRESENT STUDY

### I. Summary

In this section, this research detail the methodology, results, and implications of our research. It focusses on two key aspects: (i) the accurate estimation of aboveground carbon (AGC) density in subalpine dwarf bamboo vegetation using UAV-lidar, and (ii) the exploration of spatial clustering effects on the relationship between AGC density and environmental factors. The summarized findings and contributions of each aspect are presented below.

#### ***Appendix A: Mapping aboveground carbon density of subtropical subalpine dwarf bamboo (*Yushania niitakayamensis*) vegetation using UAV-lidar***

(Note: This manuscript has been published in *Journal of Applied Earth Observation and Geoinformation*)

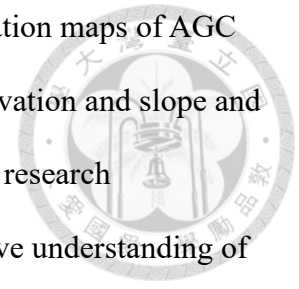
Bamboo, a widely distributed species across Asia, Central and South America, and Africa, holds significance as an effective carbon sequestration agent, with the potential for prolonged carbon fixation through its conversion into durable products like construction materials or furniture. While optical remote sensing has been extensively employed to estimate aboveground biomass (AGB) and aboveground carbon storage (AGC) in regional forests, the intricate spatial structure of bamboo impedes accurate AGC estimation using spectral features. The complexities arise from the interplay of factors such as the proportion of old and young bamboo affecting AGB and AGC and contrasting reflectance due to canopy phenology. In this context, the integration of UAV-lidar technology emerges as a solution by harnessing three-dimensional (3D) point cloud data to overcome these challenges.

This study is an in-depth exploration of accurate AGC density estimation for subalpine dwarf bamboo vegetation using UAV-lidar. This research focused on a 120-hectare research area within Tataka, Yushan National Park. By leveraging UAV-lidar point cloud data, I extracted essential lidar point cloud metrics, combined them with ground sampled data and elemental analysis, and established a robust relationship between lidar metrics and AGC density. This effort led to the development of the dwarf bamboo AGB-fresh weight relationship and the determination of a previously unavailable AGB-carbon conversion coefficient of 0.436 per AGB. This study employed five linear models to address potential multicollinearity issues among the numerous lidar metrics, including multiple stepwise regression, principle component regression, partial least square regression, elastic net regression, and multivariate adaptive regression splines (MARS). Dividing the 74 1x1 ground sample plots into training (80%) and testing (20%) sets, this study selected the MARS model based on the lowest root mean square error (RMSE) for testing data, highlighting its efficacy in mapping AGC density.

Within the MARS model, predictive variables for the height distribution of the point cloud—zmax (maximum), zq95 (95th quantile), and zq65 (65th quantile)—were identified as instrumental, revealing insights into the canopy's vertical structure. Further analysis highlighted the significant explanatory power of zq65, underscoring the importance of considering height metrics near the canopy bottom. MARS, known for establishing piecewise linear relationships, unveiled the presence of a non-linear association between AGC density and predictive variables, mirroring the complexity observed in allometry-based AGB modeling. MARS, characterized by its variable selection capability without requiring prior knowledge, proved advantageous in this study.

Leveraging MARS and the point cloud data from the open-field dwarf bamboo area,

we generated comprehensive spatial distribution and standard deviation maps of AGC density. This study unveiled a correlation between AGC density elevation and slope and terrain features by integrating contour maps and shaded relief. This research methodology promises to contribute significantly to a comprehensive understanding of the intricate spatial variability of AGC density and its potential complex interplay with environmental factors.





***Appendix B: Spatial clustering moderates the subalpine dwarf bamboo***

***AGC density on environmental gradients in a tropical island***

(Note: This manuscript will be submitted to *Advances in Bamboo Science*)



This study aimed to explore the interplay between AGC density, vegetation clustering, and environmental gradients. Specifically, the effects of high spatial resolution solar radiation, wind patterns, microtopography, and AGC density data on AGC density response were investigated. Two hypotheses guided the investigation: (H1) Vegetation spatial clustering enhances the explanation of AGC density variation compared to environmental factors alone, and (H2) the response of AGC density to environmental gradients is contingent upon spatial clustering types.

This study employed a comprehensive approach to address these hypotheses. The DSM and DEM derived from UAV-lidar point cloud data were harnessed to downscale solar irradiation, mean hourly wind speed and direction, slope, slope standard deviation, and aspect, all at a 1-meter resolution. Simultaneously, a hotspot analysis was conducted on the dwarf bamboo AGC density map from Appendix A. This analysis revealed clustering patterns, categorizing focal and neighboring grids as coldspots (clustering of low-low values), nonsignificant (clustering of low-high or high-low values), or hotspots (clustering of high-high values).

A thorough investigation was then carried out, randomly sampling 500 grids for each spatial clustering stratum to mitigate spatial autocorrelation. Utilizing a generalized additive model (GAM), this research modeled the nonlinear relationship between AGC density and spatial clustering as well as abiotic factors. The findings underscored the substantial contribution of vegetation spatial clustering in enhancing AGC density

estimation beyond the sole influence of abiotic factors. Moreover, distinct responses were unveiled within different spatial clustering types, even to the same variable. For instance, dwarf bamboo AGC density in hotspots exhibited a linear negative correlation with solar irradiation while responding nonlinearly to wind direction, wind speed and direction interaction, slope, and slope standard deviation. Conversely, AGC density in coldspots exhibited a response primarily linked to clustering, with minimal influence from abiotic factors. Notably, identifying tall-culm bamboo clusters in hotspots and short-culm clusters in coldspots suggested a distinct acclimation of dwarf bamboo to varying environmental conditions.

The study underscores the pivotal role of spatial clustering in shaping AGC density responses to environmental factors. By incorporating vegetation clustering into assessments, novel strategies for effective carbon sequestration and adaptation to climate change can be formulated. Furthermore, the findings suggest the potential of applying spatial clustering as indicators for monitoring floristic community compositional shifts in response to changing environmental conditions.

## **II. Future work**

- **Surface fire behavior simulation**

Given the wildfire risk in the Tataka area, the next step is to integrate the AGC density estimates with fine-scale digital elevation models based on the AGB-carbon conversion coefficient from Appendix A. This step facilitates simulating surface fire behavior and assesses potential wildfire impacts on the dwarf bamboo and associated tree communities. By analyzing fire spread patterns and risk zones, informed fire management strategies for ecosystem conservation and trail user

safety along popular trails can be developed.



- **Evaluation of trees and dwarf bamboo habitats selection**

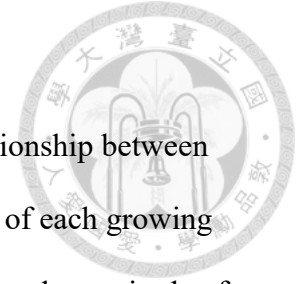
The dynamic interaction between dwarf bamboo and trees in subalpine regions, particularly regarding habitat selection (Bazzaz, 1991), has received limited attention. This aspect can illuminate the spatial distribution patterns of trees and dwarf bamboo in the face of a changing climate. Extracting point cloud data of pine, fir, and spruce trees from the UAV lidar point cloud data using the method outlined in Appendix A, the derivation of allometry functions and AGB estimates based on tree attributes obtained from ground plots follows.

This result directly compares AGB density spatial distribution between bamboo-dominated and forested areas in the subalpine landscape. Moreover, building upon the techniques elucidated in Appendix B, the intricate relationship between AGB and environmental factors within the forested zones is explored. This investigation would provides a deeper understanding of the habitat preferences and potential competitive dynamics between these two vegetation types, offering valuable insights for future management and conservation efforts.

- **Dynamics of dwarf bamboo-trees interface using UAV-lidar plot**

Expanding upon the AGC estimation method outlined in Appendix A, the research extends to the monitoring and analysis of the transitional interface between bamboo and forested areas, achieved through the utilization of the lidar plot approach (Matasci et al., 2018; Wulder et al., 2012). Initially devised for estimating forest attributes based on metrics from airborne lidar returns of specific plots and their nearest k-neighbors, this approach can be adopted to understand the

dynamics of the dwarf bamboo-trees interface.



The study intends to perform periodic validation of the relationship between AGB/AGC and point clouds within these lidar plots at the end of each growing season. This ongoing assessment aims to unravel the direction and magnitude of variations occurring within dwarf bamboo-forest interfaces over time. Furthermore, these lidar plots can serve as an adequate substitute for traditional ground sample plots, facilitating the establishment of a robust relationship between optical remote sensing data and UAV lidar features, as well as AGB/AGC density measurements.

By employing the lidar plot methodology and its application to the interface between dwarf bamboo and trees, this research provides a novel perspective on the intricate interactions shaping subalpine vegetation dynamics. The comprehensive analysis contributes to comprehending the dwarf bamboo-forest interface's spatial dynamics and ecological implications, shedding light on potential management strategies and conservation considerations.

- **Long-term dynamics of subalpine dwarf bamboo**

Exploring long-term dynamics within subalpine dwarf bamboo ecosystems constitutes a pivotal avenue for comprehensive ecological insight. Leveraging the availability of a minimum of four distinct periods of aerial imagery within the study area, a detailed analysis of sub-meter level cover changes in dwarf bamboo and the forests becomes attainable. Furthermore, the Taiwan Climate Change Projection Information and Adaptation (TCCIP) database (Lin et al., 2022) provides an extensive historical climate dataset from 1980 to 2020 at a broader scale with a resolution of 2 km, making test trends of covers of dwarf bamboo and forest

dynamic possible.

Building upon the method delineated in Appendix B, solar radiation and average wind speed are subjected to a meticulous downscaling analysis. This process unveils the nuanced impacts of solar radiation, wind speed, and micro-topography on habitat preferences and competitive interactions between dwarf bamboo and forested landscapes.

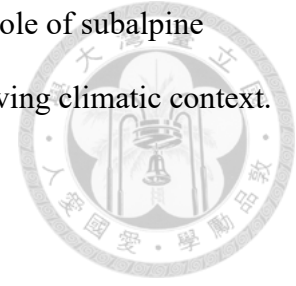
This endeavor addresses a significant gap in our present understanding, specifically concerning the process driving habitat selection and competition dynamics that have been alluded to in Appendix B. By delving into the process of how and where dwarf bamboo attains dominance, this research will contribute to a refined comprehension of the intricate processes governing the long-term dynamics of subalpine ecosystems.

- **Assessment of fog interception ability of subalpine dwarf bamboo**

The escalating impacts of climate warming have underscored the potential upslope shift of fog forests on mountainous terrains. The fog interception capability of dwarf bamboo is another water source besides the precipitation, which is predicted to be more contrasting between dry and wet seasons, and may influence the growth of the vegetation.

In light of these considerations, we propose an assessment of the fog interception capacity exhibited by the forested region and the subalpine dwarf bamboo during distinct seasons. The AGB density map was derived from the method elucidated in Appendix A. This map can be used to estimate the fog interception potential of the two distinct ecological zones once the relationship between AGB and interception

is produced. This assessment unveils pivotal insights into the role of subalpine dwarf bamboo in intercepting fog, particularly within the evolving climatic context.



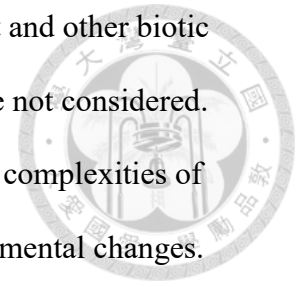
### **III. Conclusions**

This dissertation addresses several important aspects of subalpine dwarf bamboo ecosystems. The methodologies employed provide insights into estimating aboveground carbon (AGC) density and the influence of spatial clustering and environmental factors on AGC variability. The first study successfully applied UAV-lidar point cloud metrics and linear models to estimate AGC density. The findings highlight the potential of the multivariate adaptive regression splines (MARS) model for AGC density prediction. Including near canopy bottom height as a predictor underscores the importance of considering height metrics in AGC density modeling.

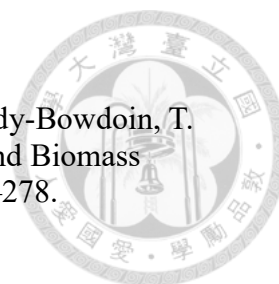
On the other hand, the second study investigated the influence of spatial clustering on AGC density and its interaction with environmental factors. The results suggest that spatial clustering significantly affects the response of AGC density to environmental gradients, emphasizing the relevance of vegetation structure in shaping dwarf bamboo's adaptation to varying environmental conditions. The contributions of this dissertation offer promising avenues for further research in the field of ecological studies and application in land management. The insights gained from the accurate AGC density estimation and consideration of spatial clustering effects can advance our understanding of dwarf bamboo ecosystems and potentially inform conservation strategies.

While the implications of this research are significant for both scientific knowledge and practical applications, it is essential to recognize the study's limitations that the

dwarf bamboo data were collected when the vegetation is dominant and other biotic factors such as potential herbivory and interaction with forests were not considered. Further research and validation are needed to fully comprehend the complexities of subalpine dwarf bamboo ecosystems and their responses to environmental changes. Additional work in this direction can shed more light on the challenges and opportunities related to climate change and biodiversity conservation in subalpine regions.



## REFERENCES



- Asner, G. P., Flint Hughes, R., Varga, T. A., Knapp, D. E., & Kennedy-Bowdoin, T. (2009). Environmental and Biotic Controls over Aboveground Biomass Throughout a Tropical Rain Forest. *Ecosystems*, 12(2), 261–278. <https://doi.org/10.1007/s10021-008-9221-5>
- Bai, S., Wang, Y., Conant, R. T., Zhou, G., Xu, Y., Wang, N., Fang, F., & Chen, J. (2016). Can native clonal moso bamboo encroach on adjacent natural forest without human intervention? *Scientific Reports*, 6(1), Article 1. <https://doi.org/10.1038/srep31504>
- Bazzaz, F. A. (1991). Habitat Selection in Plants. *The American Naturalist*, 137, S116–S130. <https://doi.org/10.1086/285142>
- Beland, M., Parker, G., Sparrow, B., Harding, D., Chasmer, L., Phinn, S., Antonarakis, A., & Strahler, A. (2019). On promoting the use of lidar systems in forest ecosystem research. *Forest Ecology and Management*, 450, 117484. <https://doi.org/10.1016/j.foreco.2019.117484>
- Bona, K., Purificação, K. N., Vieira, T. B., & Mews, H. A. (2020). Fine-scale effects of bamboo dominance on seed rain in a rainforest. *Forest Ecology and Management*, 460, 117906. <https://doi.org/10.1016/j.foreco.2020.117906>
- Caccia, F. D., Chaneton, E. J., & Kitzberger, T. (2009). Direct and indirect effects of understorey bamboo shape tree regeneration niches in a mixed temperate forest. *Oecologia*, 161(4), 771–780. <https://doi.org/10.1007/s00442-009-1412-z>
- Canavan, S., Richardson, D. M., Visser, V., Roux, J. J. L., Vorontsova, M. S., & Wilson, J. R. U. (2016). The global distribution of bamboos: Assessing correlates of introduction and invasion. *AoB Plants*, plw078. <https://doi.org/10.1093/aobpla/plw078>
- Cao, L., Coops, N. C., Sun, Y., Ruan, H., Wang, G., Dai, J., & She, G. (2019). Estimating canopy structure and biomass in bamboo forests using airborne LiDAR data. *ISPRS Journal of Photogrammetry and Remote Sensing*, 148, 114–129. <https://doi.org/10.1016/j.isprsjprs.2018.12.006>
- Chang, M.-H. (1981). Ecology and control of Yushan cane [Master Thesis]. National Taiwan University.
- Chen, Y., JY, L., & CK, W. (1992). Ecological research on high-mountain vegetation in Taiwan (II)—The variation in growth form in Yushan cane. *Yushania*, 6, 117–143.
- Chen, Y., Li, L., Lu, D., & Li, D. (2019). Exploring Bamboo Forest Aboveground



Biomass Estimation Using Sentinel-2 Data. *Remote Sensing*, 11(1), Article 1.  
<https://doi.org/10.3390/rs11010007>

da Costa, M. B. T., Silva, C. A., Broadbent, E. N., Leite, R. V., Mohan, M., Liesenberg, V., Stoddart, J., do Amaral, C. H., de Almeida, D. R. A., da Silva, A. L., Ré Y. Goya, L. R., Cordeiro, V. A., Rex, F., Hirsch, A., Marcatti, G. E., Cardil, A., de Mendonça, B. A. F., Hamamura, C., Corte, A. P. D., ... Klauberg, C. (2021). Beyond trees: Mapping total aboveground biomass density in the Brazilian savanna using high-density UAV-lidar data. *Forest Ecology and Management*, 491, 119155.  
<https://doi.org/10.1016/j.foreco.2021.119155>

Frolking, S., Palace, M. W., Clark, D. B., Chambers, J. Q., Shugart, H. H., & Hurtt, G. C. (2009). Forest disturbance and recovery: A general review in the context of spaceborne remote sensing of impacts on aboveground biomass and canopy structure. *Journal of Geophysical Research: Biogeosciences*, 114(G2).  
<https://doi.org/10.1029/2008JG000911>

Gaira, K. S., Pandey, A., Sinha, S., Badola, H. K., Lepcha, J., Dhyani, P. P., & Chettri, N. (2022). Maling bamboo (*Yushania maling*) overdominance alters forest structure and composition in Khangchendzonga landscape, Eastern Himalaya. *Scientific Reports*, 12(1), Article 1. <https://doi.org/10.1038/s41598-022-08483-8>

Gregoire, T. G., Næsset, E., McRoberts, R. E., Ståhl, G., Andersen, H.-E., Gobakken, T., Ene, L., & Nelson, R. (2016). Statistical rigor in LiDAR-assisted estimation of aboveground forest biomass. *Remote Sensing of Environment*, 173, 98–108. <https://doi.org/10.1016/j.rse.2015.11.012>

Guerreiro, C. (2014). Flowering cycles of woody bamboos native to southern South America. *Journal of Plant Research*, 127(2), 307–313.  
<https://doi.org/10.1007/s10265-013-0593-z>

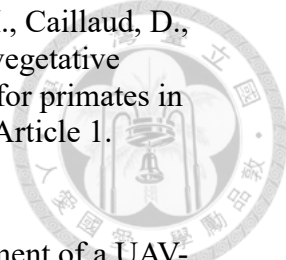
Higgins, S. I., Conradi, T., & Muhoko, E. (2023). Shifts in vegetation activity of terrestrial ecosystems attributable to climate trends. *Nature Geoscience*, 16(2), Article 2. <https://doi.org/10.1038/s41561-022-01114-x>

Hirobe, M., Miyamoto, S., Sakamoto, K., Kondo, J., Otoda, T., Akaji, Y., & Yamanaka, N. (2015). The spatial distributions of understory trees in relation to dwarf bamboo cover in a cool-temperate deciduous broadleaf forest in Japan. *Journal of Forest Research*, 20(3), 357–362.  
<https://doi.org/10.1007/s10310-015-0480-7>

Itô, H., & Hino, T. (2007). Dwarf bamboo as an ecological filter for forest regeneration. *Ecological Research*, 22(4), 706–711.  
<https://doi.org/10.1007/s11284-006-0066-0>

- Kudo, G., Amagai, Y., Hoshino, B., & Kaneko, M. (2011). Invasion of dwarf bamboo into alpine snow-meadows in northern Japan: Pattern of expansion and impact on species diversity. *Ecology and Evolution*, 1(1), 85–96. <https://doi.org/10.1002/ece3.9>
- Kudo, G., Aoshima, Y., Miyata, R., & Winkler, D. E. (2018). Altered morphologies and physiological compensation in a rapidly expanding dwarf bamboo in alpine ecosystems. *Arctic, Antarctic, and Alpine Research*, 50(1), e1463733. <https://doi.org/10.1080/15230430.2018.1463733>
- Kudo, G., Kawai, Y., Amagai, Y., & Winkler, D. E. (2017). Degradation and recovery of an alpine plant community: Experimental removal of an encroaching dwarf bamboo. *Alpine Botany*, 127(1), 75–83. <https://doi.org/10.1007/s00035-016-0178-2>
- Kumar, L., & Mutanga, O. (2017). Remote Sensing of Above-Ground Biomass. *Remote Sensing*, 9(9), Article 9. <https://doi.org/10.3390/rs9090935>
- Kuo, C.-C., Su, Y., Liu, H.-Y., & Lin, C.-T. (2021). Assessment of climate change effects on alpine summit vegetation in the transition of tropical to subtropical humid climate. *Plant Ecology*, 222(8), 933–951. <https://doi.org/10.1007/s11258-021-01152-2>
- Larperkern, P., Moe, S. R., & Totland, Ø. (2011). Bamboo dominance reduces tree regeneration in a disturbed tropical forest. *Oecologia*, 165(1), 161–168. <https://doi.org/10.1007/s00442-010-1707-0>
- Lefsky, M. A., Cohen, W. B., Harding, D. J., Parker, G. G., Acker, S. A., & Gower, S. T. (2002). Lidar remote sensing of above-ground biomass in three biomes. *Global Ecology and Biogeography*, 11(5), 393–399. <https://doi.org/10.1046/j.1466-822x.2002.00303.x>
- Lefsky, M. A., Cohen, W. B., Parker, G. G., & Harding, D. J. (2002). Lidar Remote Sensing for Ecosystem Studies: Lidar, an emerging remote sensing technology that directly measures the three-dimensional distribution of plant canopies, can accurately estimate vegetation structural attributes and should be of particular interest to forest, landscape, and global ecologists. *BioScience*, 52(1), 19–30. [https://doi.org/10.1641/0006-3568\(2002\)052\[0019:LRSFES\]2.0.CO;2](https://doi.org/10.1641/0006-3568(2002)052[0019:LRSFES]2.0.CO;2)
- Liao, M.-C., Chiu, C.-A., Lin, H.-C., Tseng, Y.-H., Tzeng, H.-Y., & Lu, K.-C. (2012). Understory vegetation diversity at *Abies kawakamii* (Hayata) Ito forest in Mt. Shei. *Quarterly Journal of Forest Research*, 34(3), 179–192.
- Liao, M.-C., Tsai, S.-T., Wang, W., Tzeng, H.-Y., & Ou, C.-H. (2013). Study on population structure of *Abies kawakamii* (Hayata) Ito in East Xue Trail of Xue Mountain. *Quarterly Journal of Forest Research*, 35(1), 1–14.

- Lin, L.-Y., Lin, C.-T., Chen, Y.-M., Cheng, C.-T., Li, H.-C., & Chen, W.-B. (2022). The Taiwan Climate Change Projection Information and Adaptation Knowledge Platform: A Decade of Climate Research. *Water*, 14(3), Article 3. <https://doi.org/10.3390/w14030358>
- Madsen, B., Treier, U. A., Zlinszky, A., Lucieer, A., & Normand, S. (2020). Detecting shrub encroachment in seminatural grasslands using UAS LiDAR. *Ecology and Evolution*, 10(11), 4876–4902. <https://doi.org/10.1002/ece3.6240>
- Matasci, G., Hermosilla, T., Wulder, M. A., White, J. C., Coops, N. C., Hobart, G. W., & Zald, H. S. J. (2018). Large-area mapping of Canadian boreal forest cover, height, biomass and other structural attributes using Landsat composites and lidar plots. *Remote Sensing of Environment*, 209, 90–106. <https://doi.org/10.1016/j.rse.2017.12.020>
- Pauli, H., Gottfried, M., Dullinger, S., Abdaladze, O., Akhalkatsi, M., Alonso, J. L. B., Coldea, G., Dick, J., Erschbamer, B., Calzado, R. F., Ghosn, D., Holten, J. I., Kanka, R., Kazakis, G., Kollár, J., Larsson, P., Moiseev, P., Moiseev, D., Molau, U., ... Grabherr, G. (2012). Recent Plant Diversity Changes on Europe's Mountain Summits. *Science*, 336(6079), 353–355. <https://doi.org/10.1126/science.1219033>
- POWO. (2023). Plants of the World Online. Facilitated by the Royal Botanic Gardens, Kew. Plants of the World Online. <http://powo.science.kew.org/taxon/urn:lsid:ipni.org:names:426782-1>
- Roussel, J.-R., Auty, D., Coops, N. C., Tompalski, P., Goodbody, T. R. H., Meador, A. S., Bourdon, J.-F., de Boissieu, F., & Achim, A. (2020). lidR: An R package for analysis of Airborne Laser Scanning (ALS) data. *Remote Sensing of Environment*, 251, 112061. <https://doi.org/10.1016/j.rse.2020.112061>
- Su, S. J. (1985). Studies on the climate and vegetation types of the natural forests in Taiwan.(III). A scheme of geographical climatic regions. *Quarterly Journal of Chinese Forestry*, 18(3), 33–44.
- Takano, K. T., Hibino, K., Numata, A., Oguro, M., Aiba, M., Shiogama, H., Takayabu, I., & Nakashizuka, T. (2017). Detecting latitudinal and altitudinal expansion of invasive bamboo *Phyllostachys edulis* and *Phyllostachys bambusoides* (Poaceae) in Japan to project potential habitats under 1.5°C–4.0°C global warming. *Ecology and Evolution*, 7(23), 9848–9859. <https://doi.org/10.1002/ece3.3471>
- Tomimatsu, H., Yamagishi, H., Tanaka, I., Sato, M., Kondo, R., & Konno, Y. (2011). Consequences of forest fragmentation in an understory plant community: Extensive range expansion of native dwarf bamboo. *Plant Species Biology*, 26(1), 3–12. <https://doi.org/10.1111/j.1442-1984.2010.00310.x>

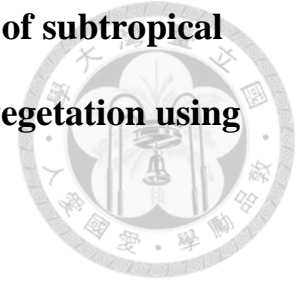
- 
- van der Hoek, Y., Emmanuel, F., Eckardt, W., Kwizera, I., Derhé, M., Caillaud, D., Stoinski, T. S., & Tuyisingize, D. (2019). Recent decline in vegetative regeneration of bamboo (*Yushania alpina*), a key food plant for primates in Volcanoes National Park, Rwanda. *Scientific Reports*, 9(1), Article 1. <https://doi.org/10.1038/s41598-019-49519-w>
- Wallace, L., Lucieer, A., Watson, C., & Turner, D. (2012). Development of a UAV-LiDAR System with Application to Forest Inventory. *Remote Sensing*, 4(6), 1519–1543. <https://doi.org/10.3390/rs4061519>
- Wang, D., Wan, B., Qiu, P., Zuo, Z., Wang, R., & Wu, X. (2019). Mapping Height and Aboveground Biomass of Mangrove Forests on Hainan Island Using UAV-LiDAR Sampling. *Remote Sensing*, 11(18), Article 18. <https://doi.org/10.3390/rs11182156>
- Wang, D., Xin, X., Shao, Q., Brolly, M., Zhu, Z., & Chen, J. (2017). Modeling Aboveground Biomass in Hulunber Grassland Ecosystem by Using Unmanned Aerial Vehicle Discrete Lidar. *Sensors (Basel, Switzerland)*, 17(1). <https://doi.org/10.3390/s17010180>
- Winkler, D. E., Amagai, Y., Huxman, T. E., Kaneko, M., & Kudo, G. (2016). Seasonal dry-down rates and high stress tolerance promote bamboo invasion above and below treeline. *Plant Ecology*, 217(10), 1219–1234. <https://doi.org/10.1007/s11258-016-0649-y>
- Wu, K.-S., & Kao, W.-Y. (2021). Phenotypic plasticity and genetic variation in leaf traits of *Yushania niitakayamensis* (Bambusoideae; Poaceae) in contrasting light environments. *Journal of Plant Research*. <https://doi.org/10.1007/s10265-021-01327-y>
- Wulder, M. A., White, J. C., Bater, C. W., Coops, N. C., Hopkinson, C., & Chen, G. (2012). Lidar plots — a new large-area data collection option: Context, concepts, and case study. *Canadian Journal of Remote Sensing*, 38(5), 600–618. <https://doi.org/10.5589/m12-049>
- Xu, Q.-F., Liang, C.-F., Chen, J.-H., Li, Y.-C., Qin, H., & Fuhrmann, J. J. (2020). Rapid bamboo invasion (expansion) and its effects on biodiversity and soil processes +. *Global Ecology and Conservation*, 21, e00787. <https://doi.org/10.1016/j.gecco.2019.e00787>
- Ye, X.-Y., Ma, P.-F., Yang, G.-Q., Guo, C., Zhang, Y.-X., Chen, Y.-M., Guo, Z.-H., & Li, D.-Z. (2019). Rapid diversification of alpine bamboos associated with the uplift of the Hengduan Mountains. *Journal of Biogeography*, 46(12), 2678–2689. <https://doi.org/10.1111/jbi.13723>
- Younginger, B. S., Sirová, D., Cruzan, M. B., & Ballhorn, D. J. (2017). Is biomass a reliable estimate of plant fitness?1. *Applications in Plant Sciences*, 5(2).

<https://doi.org/10.3732/apps.1600094>

Yuen, J. Q., Fung, T., & Ziegler, A. D. (2017). Carbon stocks in bamboo ecosystems worldwide: Estimates and uncertainties. *Forest Ecology and Management*, 393, 113–138. <https://doi.org/10.1016/j.foreco.2017.01.017>



**APPENDIX A. Mapping aboveground carbon density of subtropical  
subalpine dwarf bamboo (*Yushania niitakayamensis*) vegetation using  
UAV-lidar**



**This manuscript is published in *Journal of Applied Earth Observation and  
Geoinformation*.**

Pan, H.-L., et al. (2023). "Mapping aboveground carbon density of subtropical  
subalpine dwarf bamboo (*Yushania niitakayamensis*) vegetation using UAV-lidar."

International Journal of Applied Earth Observation and Geoinformation 123: 103487.

Hsiao-Lung Pan<sup>a,b</sup>, Chu-Mei Huang<sup>c</sup>, Cho-ying Huang<sup>a</sup>

<sup>a</sup>Department of Geography, National Taiwan University, Taipei 10617, Taiwan

<sup>b</sup>Technical Service Division, Taiwan Forestry Research Institute, Taipei 10066,  
Taiwan

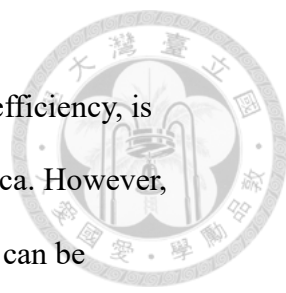
<sup>c</sup>Silviculture Division, Taiwan Forestry Research Institute, Taipei 10066, Taiwan

Corresponding author: Cho-ying Huang (e-mail: [choying@ntu.edu.tw](mailto:choying@ntu.edu.tw))

Address: 1 Sec. 4, Roosevelt Rd., Taipei, Taiwan 10617

Phone: +886-2-3366-3733; Fax: +886-2-2362-2911

## Abstract



Bamboo, a fast-growing vegetation with high carbon sequestration efficiency, is widely distributed across Asia, Central and South America, and Africa. However, mapping aboveground carbon (AGC) density ( $\text{kgC m}^{-2}$ ) in bamboo can be challenging due to the changing composition of old and new culms or the phenology of the canopy. In this study, we conducted a UAV-lidar survey on 120 ha of subalpine dwarf bamboo (*Yushania niitakayamensis*) vegetation in Central Taiwan. We destructively collected dwarf bamboo plants from seventy-four  $1 \times 1$  m plots and derived 64 spatially corresponding lidar height and density distribution metrics to model dwarf bamboo AGC density. We applied five regression models (stepwise linear regression, principal component regression, partial least squares regression, elastic net, and multivariate adaptive regression splines [MARS]) to model dwarf bamboo AGC density. MARS outperformed other models by referring to model residuals. The metrics  $z_{\max}$  (maximum of lidar return height distribution),  $z_{q95}$  (95th percentile), and  $z_{q65}$  (65th percentile) were salient variables ( $p < 0.001$ ), especially  $z_{q65}$ , suggesting that the conventional model specification of height percentiles of the canopy top might overlook that near the canopy bottom or might be due to insufficient point density. Finally, we used MARS to map the dwarf bamboo AGC density of the study area. We found that AGC spatial variation in dwarf bamboo may be related to topographic characteristics and/or microclimate. This study proposes a regression model to integrate UAV-lidar metrics for precise subalpine dwarf bamboo carbon density mapping, aiding regional spatial carbon-cycle monitoring.

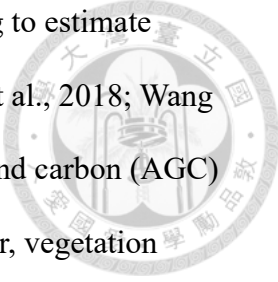
**Keywords:** aboveground biomass, biomass-carbon conversion, canopy lidar metrics, multivariate adaptive regression splines (MARS), topography

## 1. Introduction

Bamboo is a fast-growing plant with high carbon-storage efficiency (Yuen et al., 2017) that is widely distributed in Asia, Central and South America, and Africa (Lobovikov et al., 2007; Bystriakova et al., 2004, 2003) and ranges from lowlands to mountains (Scurlock et al., 2000). It can adapt to environmental change (Kudo et al., 2011; Takano et al., 2017; Winkler et al., 2016) or rapidly recover after disturbance (Safford, 2001). In addition, bamboo is also an environmentally friendly material and sequesters carbon for a long time once it becomes a durable product or construction material (Kumar & Mandal, 2022; Vogtländer et al., 2010). The desirable fuel characteristics and short rotation of harvest also make bamboo an important bioenergy source compared to other biomass feedstocks (Akinlabi et al., 2017; Liu et al., 2014; Engler et al., 2012; Scurlock et al., 2000).

It is challenging to map regional three-dimensional (3D) attributes (e.g., carbon storage) of bamboo vegetation due to the complexity of the vegetation structure (Chen et al., 2019). Colonial plants such as bamboo form a positive growth feedback loop between their above- and belowground parts. Belowground rhizomes store resources from aboveground shoots to extend their territory via the growth of rhizomes, which produce new culms (McClure, 2013). As the number of culms increases, the diameter of new growth tends to be smaller; as the number of culms decreases, the diameter is larger. In addition, the declining specific gravity of old culms decreases the AGB density. Hence, carbon storage fluctuates with new growth and old culms (Lobovikov et al., 2012). This is in contrast to arborescent forests in which carbon storage can be precisely modeled using stem diameter and/or canopy height (Chave et al., 2003; Réjou-Méchain et al., 2017).





Previous research efforts have used passive optical remote sensing to estimate bamboo aboveground biomass (AGB) (Venkatappa et al., 2020; Li et al., 2018; Wang et al., 2021; Patil et al., 2012), which can be converted to aboveground carbon (AGC) by multiplying by a biomass-carbon conversion coefficient. However, vegetation phenology may alter bamboo canopy reflectance, but carbon storage remains stable (Chen et al., 2019), limiting the use of optical remote sensing for this task. Airborne light detection and ranging (lidar) delineates the 3D profile of the bamboo canopy structure utilizing the height and intensity of pulse returns to bypass the mentioned issue (Cao et al., 2019). However, the approach is costly, and an unmanned aerial vehicle (UAV) lidar system could be an ideal alternative (Beland et al., 2019). UAV-lidar has been applied to estimate the AGB of different vegetation types, including tropical forests (d'Oliveira et al., 2020; Wang et al., 2019), savannas (da Costa et al., 2021) and grasslands with and without the presence of shrubs (Madsen et al., 2020; Wang et al., 2017; Zhao et al., 2021), using lidar-derived metrics. However, to our knowledge, no study has utilized UAV-lidar to map bamboo AGC. Therefore, the objective of this study is to assess the feasibility of using UAV-lidar derived canopy structural variables for regional mapping of the AGC density (e.g., kgC m<sup>-2</sup>) in bamboo vegetation.

## 2. Materials and Methods

### 2.1. Study area

We conducted the study in 120 ha of dwarf bamboo vegetation (*Yushania niitakayamensis*) located on the Tataka Saddle in Yushan National Park of Central Taiwan (Fig.1). It is a representative subalpine vegetation in Taiwan. The annual precipitation and temperature are 2378 mm y<sup>-1</sup> and 10 °C, respectively (Chiang &

Chang, 2010). Dwarf bamboo, Taiwan red pine (*Pinus taiwanensis*), and Masters pine (*Pinus armandii* var. *mastersiana*) are dominant on southern slopes, and hemlock (*Tsuga chinensis* var. *formosana*), spruce (*Picea morrisonicola*), and dwarf bamboo are present on northern slopes (Fig. 1b). The relief of the Tataka Saddle ranges from 2610 to 2881 m a.s.l. Based on our field knowledge, the culms in dwarf bamboo vegetation were estimated to be approximately 1–5 years old with a culm density of 62–276 m<sup>-2</sup>. Dwarf bamboo produces new shoots in March and April, and AGB reaches a maximum in August and September and slightly declines at the end of the growing season (November). During the growing season, the allocation of resources between leaves/branches and culms fluctuates. However, after November, the AGB stabilizes (Chen, 1983).

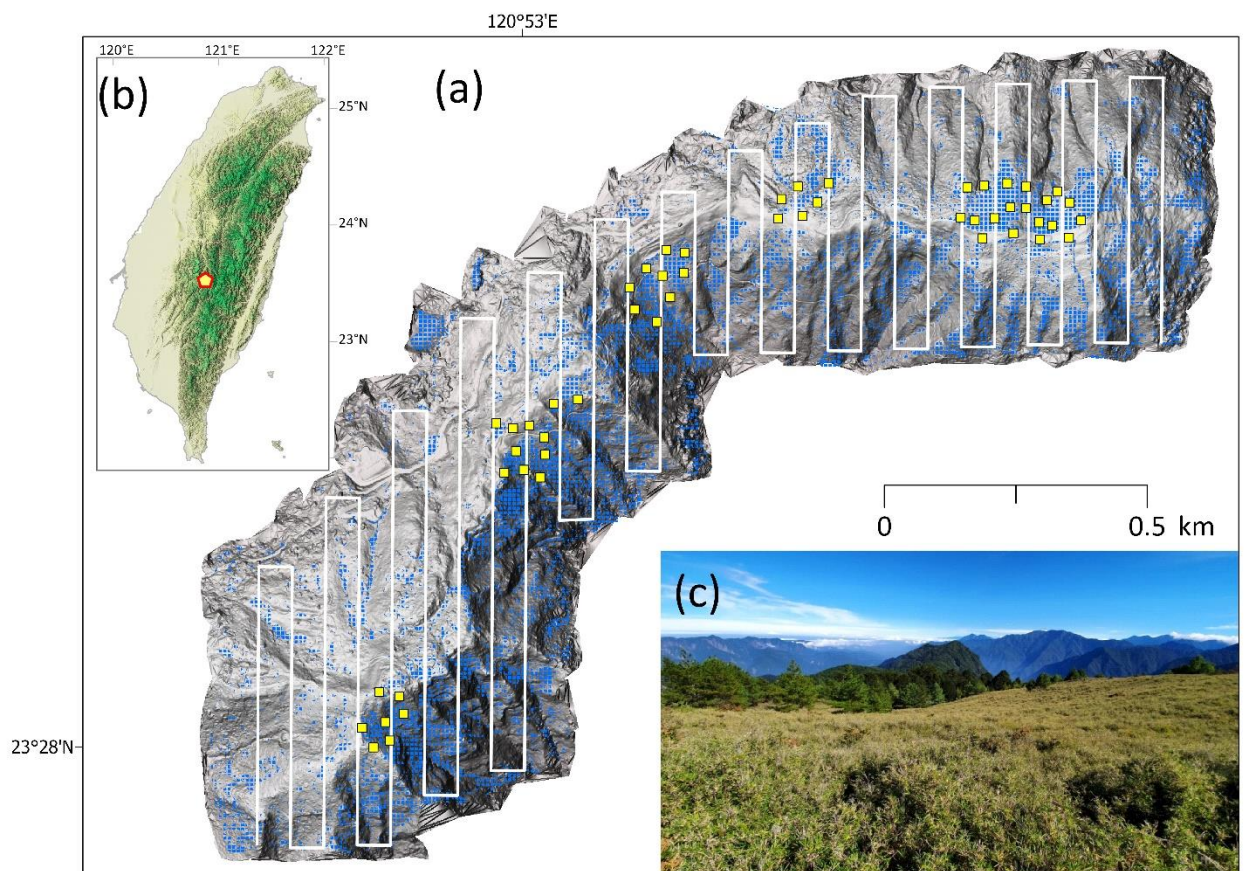
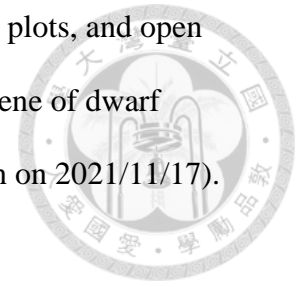


**Fig. 1.** (a) The study area Tataka located in the subtropical subalpine vegetation zone in (b) Central Taiwan (the yellow pentagon). White lines, yellow squares and blue

square dots are unmanned aerial vehicle (UAV) flight lines, sample plots, and open dwarf bamboo vegetation spatial distribution, respectively. (c) A scene of dwarf bamboo vegetation in Tataka (photograph taken by Hsiao-Lung Pan on 2021/11/17).



## 2.2. UAV-lidar point-cloud acquisition

The UAV-lidar analyses of this study consisted of lidar data acquisition, processing, extracting metrics, and model fitting (see Fig. 2 for the workflow and Fig. 3a). The lidar field campaign was carried out on November 17–19, 2021. The lidar system (gAirHawk GS-130X, Wuhan Geosun Navigation Technology, Wuhan, China) was mounted on a UAV (Matrice 300, DJI, Shenzhen, China), which received two discrete returns. Flight lines were in a north-south direction across an east-west ridge, and the UAV flew along the terrain, maintaining a height of 82 meters above the ground based on a 20-m resolution digital elevation model (DEM) provided by Ministry of Digital Affairs, Taiwan with a controlling speed of 7.2–8 m s<sup>-1</sup> (Fig. 1) so the lidar system can acquire dense point cloud. Moreover, we programmed the flight with a 30% side overlap to reduce noise in border area of swaths.

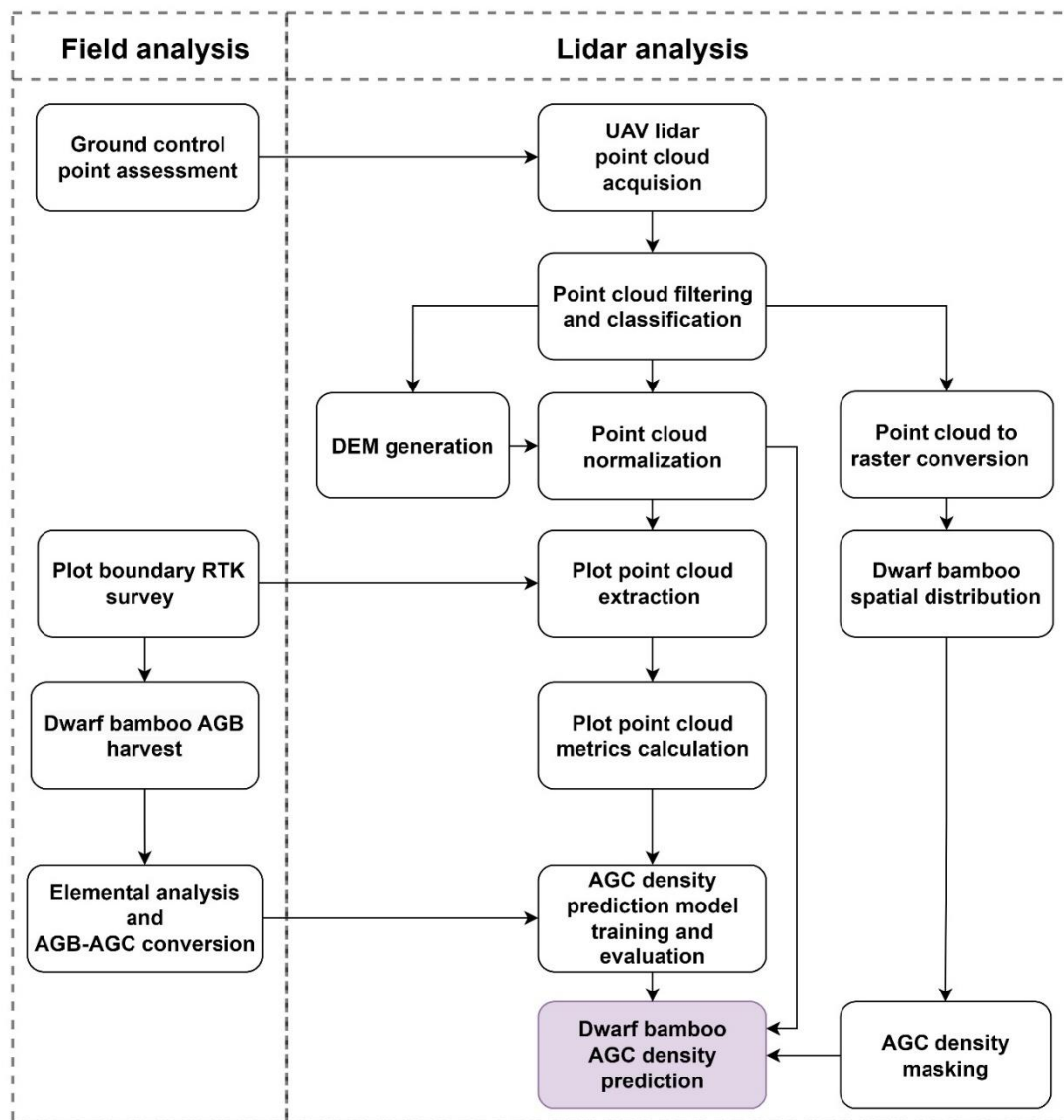


**Fig. 2.** The work process of estimating dwarf bamboo aboveground carbon (AGC) density through the integration of UAV-lidar and field analysis. The shaded box represents the final outcome of these analyses.

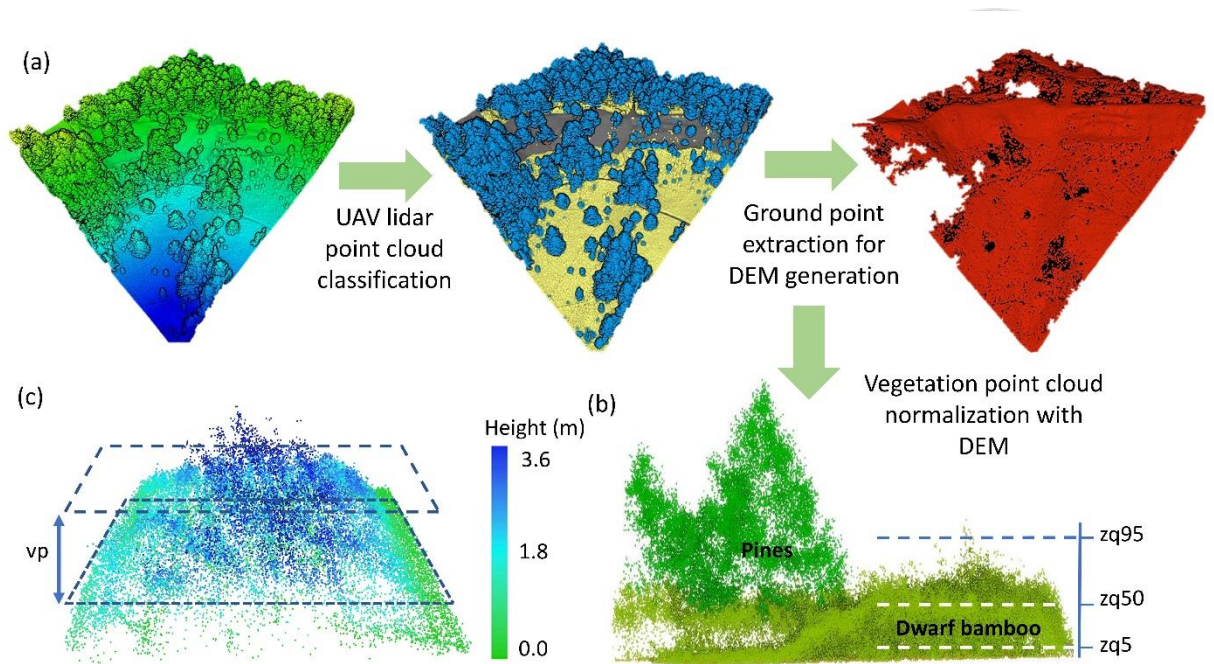
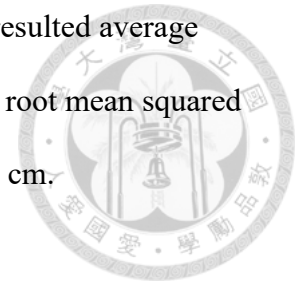


**Fig. 3.** (a) Lidar point-cloud processing before extracting lidar metrics of vegetation structural characteristics. (b) Dwarf bamboo plot lidar metrics of the 95<sup>th</sup>, 50<sup>th</sup>, and 5<sup>th</sup> percentiles (zq95, zq50 and zq5, respectively). (c) The metric vp is the percentage of lidar returns that fall between the 19<sup>th</sup> and lower equal-depth layers.

When the GNSS (global navigation satellite system) unit of the lidar system received the satellite position signals, a GNSS receiver (RTK-K500, Kang Ying Enterprise Ltd., New Taipei City, Taiwan, with horizontal and vertical accuracies of  $\pm 2.5 \text{ mm} + 0.5 \text{ ppm}$  and  $\pm 5 \text{ mm} + 0.5 \text{ ppm}$ , respectively, in a static mode) was also installed in the study area as a base station for lidar GNSS signal correction. After the completion of lidar data acquisition, a post-processed kinematic procedure was applied to correct the UAV-lidar GNSS signals and compute the lidar point-cloud coordinates. Since the height measurement of ground lidar points influences the quality of the DEM, we assessed the accuracy of the ground elevation of the processed lidar data. We surveyed the ground control points in the study area with the real-time kinematic (RTK) receiver with horizontal and vertical accuracies of  $\pm 8 \text{ mm}$

+ 1 ppm and  $\pm 15$  mm + 1 ppm, respectively, in a RTK mode. The resulted average UAV lidar point-cloud density was  $388.3 \pm 66.6$  points  $m^{-2}$ , and the root mean squared error of the ground control point ground elevation was less than 1.5 cm.

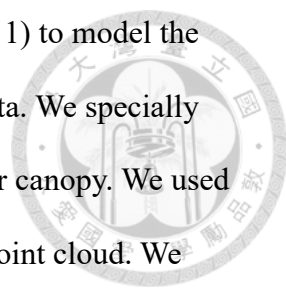


### 2.3. Field AGC density measurement

We sampled 74 randomly distributed  $1 \times 1$  m dwarf bamboo plots (Fig. 1a) right after the UAV-lidar acquisition; each plot was at least 6–15 m away from other plots. We used a polyvinyl chloride frame to outline each plot boundary, harvested all aboveground tissues, and weighed the fresh parts in kilograms to a second decimal place. We also positioned the boundary of each plot with the RTK GNSS receiver to extract UAV-lidar point-cloud data. We then randomly selected a subsample of 3–5 fresh dwarf bamboo plants in each plot, stored them in a zipper-top bag, and weighed the fresh weights in grams to a second decimal place and oven-dried them in a laboratory for 72+ h at 80 °C. We then calculated the dry and fresh-weight ratio of each subsample, applied the ratio to the fresh weight of the plot, and calculated AGB density. We also randomly selected 20 individuals to estimate the carbon content of dwarf bamboo. Since the percentages of oven-dried weight of leaves and non-leaf parts (branches and culms) may be different (Chen, 1983), we ground these parts separately using a vibrating sample mill (TI-100, CMT Co., LTD., Fukusima, Japan) to pass through a 0.177-mm sieve (80 mesh). The samples were analyzed by a combustion method using a CHNS analyzer (Elementar vario EL III, Elementar Analysensysteme GmbH, Hanau-Germany) by referring to Dhaliwal et al.(2014). Finally, with the knowledge AGB density ( $kg\ m^{-2}$ ) and the AGB-carbon conversion coefficient, we calculated the AGC density ( $kgC\ m^{-2}$ ).

### 2.4. Lidar point-cloud processing and metric extraction





In this study, we generated a comprehensive set of metrics (Table 1) to model the dwarf bamboo AGC density derived from UAV-lidar point-cloud data. We specially focused on the open dwarf bamboo vegetation found in the top-layer canopy. We used both first and second lidar returns to facilitate classification of the point cloud. We first filtered the point cloud into ground points and non-ground points using Lidar360 v. 5 (Green Valley International, Berkeley, California, USA), which employed an improved progressive triangulated irregular network densification filtering algorithm (Zhao et al., 2016). The classified ground points were used to interpolate a 1-m DEM of the study area. To extract the dwarf bamboo point cloud, we classified the non-ground points into three categories: high vegetation, low vegetation (dwarf bamboo), and non-vegetation. This classification was achieved using the built-in machine learning function (random forests) of the software. The training sample for the point cloud classification was manually selected from multiple  $100 \times 100$  m non-ground point-cloud tiles containing the field plots, and each point was assigned to one of the three vegetation classes. After training the classification model, we applied it to the entire point cloud in the study area. To ensure accuracy, we thoroughly inspected and corrected the outcome of the point-cloud classification. Next, we normalized the classified point cloud by subtracting the DEM from the point cloud. This process provided us with the height information of vegetation and other object point clouds regardless of their elevations. We also mapped the dwarf bamboo vegetation spatial distribution by extracting the low vegetation (dwarf bamboo) from the entire classified point cloud and converted it to a 1-m resolution raster. This raster served as the mask for generating a dwarf bamboo AGC density map (Fig. 2). Finally, we imported the normalized point-cloud data into the R package lidR (Roussel et al., 2020) and extracted point cloud within the boundaries of every field plot, which had

been measured by the RTK survey. Subsequently, we computed various lidar metrics in lidR. These metrics include standard statistical and cumulative percentage metrics, resulting in a total of 64 height- and intensity-related metrics to model the variation in AGC density (Table 1).

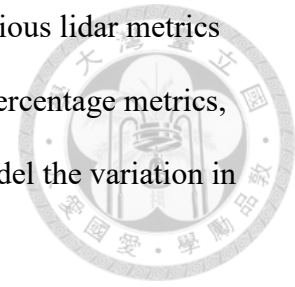


**Table 1.** Lidar metrics used as model predictors and corresponding descriptions.

Lidar metrics	Description
zmax, zmean, zmin	Maximum, mean, and minimum of height of point cloud.
zsd, zskew, zkurt, zrange	Standard deviation, skewness, kurtosis and range of height distribution.
pzabovemean	Percentage of height distribution above zmean value.
zq95, zq90, ..., zq5	95 <sup>th</sup> , 90 <sup>th</sup> , ..., 5 <sup>th</sup> percentile of height distribution.
zpcumx	Cumulative percentage of point cloud in x <sup>th</sup> equal depth layer of 20, where x is 1 to 19.
imax, imean, isd, iskew, ikurt	Descriptive statistics of intensity distribution of point cloud.
itot	Sum of return intensity
ipcumzqk	Percentage of intensity returned below the kth percentile of height, where k =10, 30, 50, 70, 90.
area, n, p1th and p2th	Area of a plot, number of lidar returns in a plot, and percentage of first return and second return.
entropy <sub>sH</sub>	Entropy of scaled height distribution.
vp	Percentage of point cloud between 19 <sup>th</sup> and 13 <sup>th</sup> layer. (see eq.2 and 3)
Rumple index	The Rumple index of top surface of point cloud.

Among these metrics, entropy, cumulative percentage of returns along canopy



vertical profiles (Asner et al., 2009) and a surface roughness index were utilized to estimate dwarf bamboo density. Due to the height variation of dwarf bamboo (from < 1 to 5 m), the entropy of dwarf bamboo was calculated based on slices relative to its height rather than constant intervals. Therefore, we modified the entropy to a scaled height version ( $entropy_{sH}$ ), which sliced the point cloud within a plot into 20 even-depth layers, counted the number of lidar returns  $n_i$  in each layer, calculated the entropy, and standardized the entropy with the maximum entropy.  $entropy_{sH}$  of a plot reaches a maximum if all layers have the same amount of returns, meaning that the reference proportion ( $p_{ref}$ ) is 1/20 (eq.1), and was calculated by the “entropy” function in the lidR package (Roussel et al., 2020).

$$Entropy_{sH} = \frac{-\sum_1^{20} p_i \times \log(p_i)}{-\sum_1^{20} p_{ref} \times \log(p_{ref})}, p_i = \frac{n_i}{\sum_1^{20} n_i}; p_{ref} = 1/20 \quad (1)$$

Since the portion of returns in canopy of varying size may be linked to AGC density across plots. To determine which portion explained the AGC the best, in this study, we proposed a new metric “volumetric percentage of returns (vp)” in a given area between the 19th and a lower layer (eqs. 2 and 3, Fig. 3c). Finally, the roughness of the top surface of the lidar point cloud could also be related to the heterogeneity of the canopy structure (Karna et al., 2020), which might be able to explain the variation in AGC density. The Rumble index, a measure of roughness, was the quotient of the top surface area of the lidar point cloud and the projected ground area and was calculated by the “rumple” function in the lidR package.

$$i^* = \underset{i}{\operatorname{argmax}} [corr((zpcum_{19} - zpcum_i), AGC)], i = 1, 2, \dots, 18 \quad (2)$$

$$vp = zpcum_{19} - zpcum_{i^*} \quad (3)$$

## 2.5. AGC density modeling

Linear models can predict AGC density without prior knowledge on the nature of the relationship to be developed but they have to address predictor selection and issues of large variance of parameter estimates arising from the excessive number of predictors. When the number of predictors is greater than the sample size, it may decrease the AGC estimate stability (Harrell, 2015). Meanwhile, the multicollinearity among lidar metrics could also decrease model prediction accuracy (James et al., 2021). Hence, we employed models that mitigate the impact of an excessive number of predictors and potential multicollinearity among them. These include stepwise linear regression (SLR), principal component regression (PCR), partial least square regression (PLS), the elastic net algorithm and multivariate adaptive regression splines (MARS). We realized that machine learning has been a prevailing tool for this type of application. However, the small plot size and limited sample size owing to intensive labor and the restricted amount of harvest in the National Park constrained our use of tree-based or nonparametric methods (Zeng et al., 2019; Han et al., 2019), and the interpretability of linear models could be relatively straightforward. Stepwise linear regression utilizes forward and backward selection to find the subset of predictors that are not highly correlated (James et al., 2021; Zhao et al., 2021). Instead of inclusion and exclusion of SLR, PCR and PLS use principal components as new predictors that are linear compositions of the original lidar metrics to reduce the number of predictors and multicollinearity issues (Huang et al., 2019, 2023; Lai et al., 2021). These methods regress the response variable on the first few significant principal components and have been applied to reduce the dimension of predictors and result in a brief and accurate model for prediction (James et al., 2021). In contrast to composite new predictors, elastic net, a combination of ridge and LASSO



regression, forces most regression coefficients close to or directly to zero. Elastic net may lead to biased estimates of parameters, but it gains overall accuracy with a small subset of predictors and identifies the predictors contributing the largest prediction accuracy. Extending from the global linear relationship between the response variable and predictors, MARS comprises piecewise linear basis functions, also known as linear splines (Hastie et al., 2009). The basis functions of a predictor are created by dividing the domain of the predictor with knots. Each basis function is responsible for capturing the local trend of the response variable. Furthermore, MARS can incorporate interactions between two or more basis functions into the model to increase fitting performance. Thus, MARS is flexible in describing the non-linearity of the response variable while excluding the linear interdependency of predictors.

These regression models all required choosing hyperparameters (numbers of predictors [components] for SLR, PCR, and PLS, coefficients for regularization penalty functions for elastic net, and number of basis functions and degree of interactions for MARS) with cross-validation to determine the best model that avoids dependency and has the highest AGC density prediction accuracy among others. We partitioned the 74 field AGC density samples into training (80%,  $n = 62$ ) and test (20%,  $n = 12$ ) data of similar distribution using the “caret” package in R (Kuhn et al., 2022). We selected the root mean square error (RMSE) to determine the best-tuned hyperparameters. We adopted a 10-fold cross-validation in “caret” on training data to find the best-tuned hyperparameters for each model type. We then used the best-tuned hyperparameters to fit the model to the training data (Kuhn et al., 2022). The hyperparameter for SLR is the maximum number of predictors to include in the model. We followed the rule of thumb that the ratio of the number of predictors to the sample size is less than 1/15 (Harrell, 2015) and set the hyperparameter from 2 to 5 in

the “train” function in the caret package. The “train” function suggested the best value for the hyperparameter of SLR and returned the corresponding fitted result. PCR produced principal components by singular value decomposition, while PLS fit the model with the kernel algorithm proposed by Dayal & MacGregor (1997). The objective function of elastic net (eq. 4) (Hastie et al., 2021; Friedman et al., 2010) shows that the hyperparameter alpha controls the penalty and determines whether it is lasso regression (alpha = 1), ridge regression (alpha = 0), or a mixture of both, while lambda controls the strength of the penalty. We used the “glmnet” method in the training function and tuned with 20 alpha and 20 lambda values.

$$\min_{(\beta_0, \beta) \in \mathbb{R}^{p+1}} \frac{1}{2n} \sum_1^n (AGC_i - \beta_0 - \beta x_i^T)^2 + \lambda [(1 - \alpha) \|\beta\|_2^2 / 2 + \alpha \|\beta\|_1] \quad \text{where}$$

$$0 \leq \alpha \leq 1, 0 \leq \lambda, \|\beta\|_2 = \sqrt{\sum_1^p \beta_j^2}, \|\beta\|_1 = |\sum_1^p \beta_j|, \text{ and } x_i \in \mathbb{R}^p \text{ are}$$

observations (4)

The basis functions of MARS are called terms when implemented in the caret package and earth package (Milborrow, 2021). It creates a full basic matrix of terms and their multiplication and adds one term at a time until the maximum number of terms is reached or the improvement saturates in the forward pass. It excludes the term iteratively and generates the corresponding smaller sub-models until the intercept is left and finds the subset with the best generalized cross-validation in the backward pass step. Cross-validation was applied to find the best number of terms and degree of interaction.

We identified the model for future prediction by comparing the RMSEs (eq. 5, where  $i$  is the index number of an observation and  $n$  is the number of observations) on training and test datasets and selected the model with the lowest RMSE once we fitted models on the training dataset with respectively tuned hyperparameters (Kuhn, 2019).

The trained models that have relatively low RMSEs in both datasets have better bias-variance tradeoffs and perform well in future prediction (James et al., 2021). In addition to RMSE, we also listed the nRMSE (normalized root mean square error, eq. 6, where  $sd$  is the standard deviation of observations), MAE (mean absolute error, eq. 7), and MAPE (mean absolute percentage error, eq. 8) on both training and test data. Apart from the overall performance metrics, we additionally compared the distribution of residuals on the test data to understand how well the trained models perform for future prediction.

$$RMSE = \sqrt{n^{-1} \sum_1^n (AGC_i - \widehat{AGC}_i)^2} \quad (5)$$

$$nRMSE = sd^{-1} \sqrt{n^{-1} \sum_1^n (AGC_i - \widehat{AGC}_i)^2} \quad (6)$$

$$MAE = n^{-1} \sum_1^n |AGC_i - \widehat{AGC}_i| \quad (7)$$

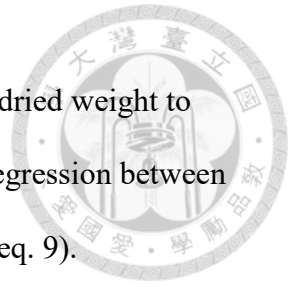
$$MAPE = n^{-1} \sum_1^n \frac{|AGC_i - \widehat{AGC}_i|}{AGC_i} \times 100\% \quad (8)$$

Once we determined the best AGC density model for the subalpine dwarf bamboo vegetation, we employed the vip package (Greenwell et al., 2020) to investigate the important UAV-lidar predictors based on model-specific importance scores. We then mapped the AGC density and the variation ( $sd$ ) of the study region using  $1 \times 1$  m resolution lidar returns and the “pixelmetrics” function in lidR with best model. We used dwarf bamboo vegetation spatial distribution map to extract the dwarf bamboo AGC density distribution.

### 3. Results

### 3.1. Dwarf bamboo AGC

The 74 oven-dried subsamples were used to compute the ratio of dried weight to fresh weight and AGB density of the plots. We also developed the regression between subsample fresh weight (FW) and oven-dried weight (DW) (Fig. 4, eq. 9).



$$DW = 0.873 + 0.518FW \quad R_{adj}^2 = 0.985 \quad (9)$$

The sample mean ( $\pm$  standard error [SE]) percentage of leaf dry weight was  $19.79 \pm 1.86\%$ , and that of the non-leaf part was  $80.21 \pm 1.86\%$ . The mean ( $\pm$  SE) carbon content of the leaf sample was  $0.419 \pm 0.002$ , and that of the non-leaf part was  $0.44 \pm 0.001$ , and the carbon content of the non-leaf part was distributed more compactly than that of the leaf part (Fig. 4). Paired t tests showed that leaf and non-leaf carbon contents were significantly different ( $p < 0.001$ ). The sample mean ( $\pm$  SE) AGB-carbon conversion coefficient was  $0.436 \pm 0.01$ .

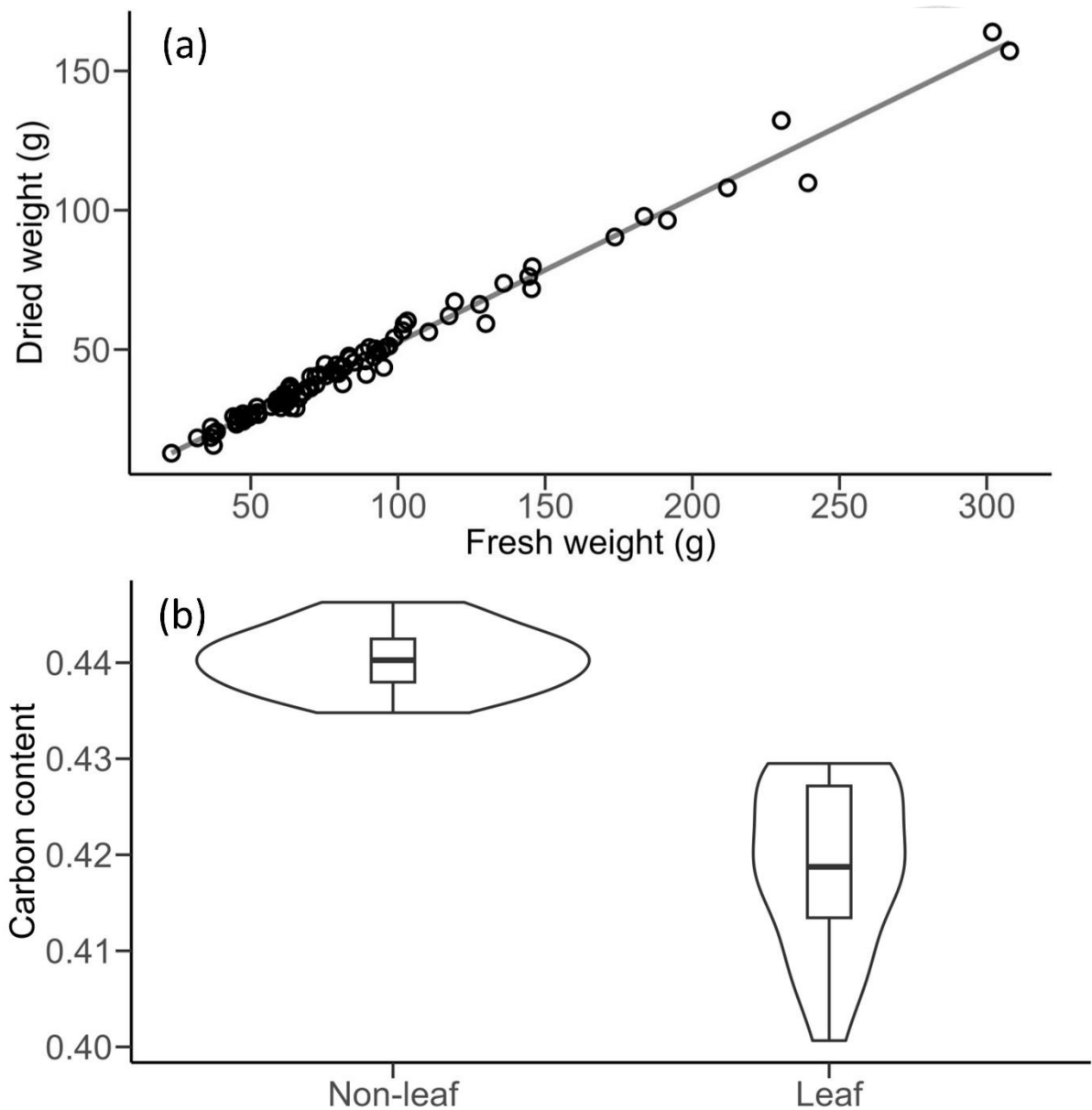


**Fig. 4.** (a) Relationships between dwarf bamboo fresh and oven-dried weights; (b) carbon content of leaves and non-leaf (branches and culms) parts. These two groups were significantly different ( $p < 0.001$ ).

### 3.2. UAV-lidar AGC density estimation models

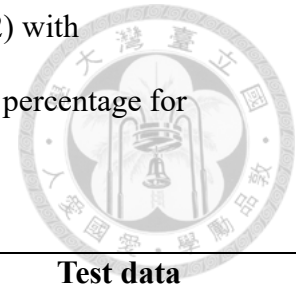
We set the max number of predictors in SLR to five, following the rule of thumb of 1/15, while cross-validation suggested that the tuned number of predictors should be four. SLR estimates fitted with training data were significant ( $p < 0.01$ ) except for the intercept ( $p = 0.412$ ). Tuning of PCR suggested the number of PCs to be 11, which

explained 100% and 54.81% of the variance of all predictors and AGC density in the training data, respectively. In contrast, tuning the PLS resulted in explaining 100% and 48.78% of the variance in the predictors and AGC density, respectively, with six components. Tuning of elastic net showed the use of best-tuned alpha (0.10) and lambda (0.14) in the model, which included 31 nonzero estimates of predictors.

Finally, the number of terms and degree of interaction for the MARS model were 4 and 1, respectively. Comparing the best-tuned outcomes (Table 2), we conclude that the performance of MARS is superior to that of the other models, yielding the smallest RMSE and nRMSE and second lowest MAE and MAPE on the test data.



**Table 2.** Model evaluation on training (n = 62) and test data (n = 12) with performance measures ( $\text{kgC m}^{-2}$  for RMSE, nRMSE and MAE and percentage for MAPE).



Predictors		Training data				Test data			
		RMSE	nRMSE	MAE	MAPE	RMSE	nRMSE	MAE	MAPE
Model									
SLR	4	0.166	0.700	0.133	22.22	0.169	0.542	0.119	19.34
PCR	11	0.158	0.667	0.127	22.34	0.170	0.545	0.139	23.40
PLS	6	0.168	0.709	0.133	23.46	0.169	0.542	0.145	26.03
Elastic net	31	0.158	0.667	0.128	21.93	0.174	0.558	0.135	22.30
MARS	4	0.164	0.692	0.128	22.67	0.150	0.481	0.123	20.71

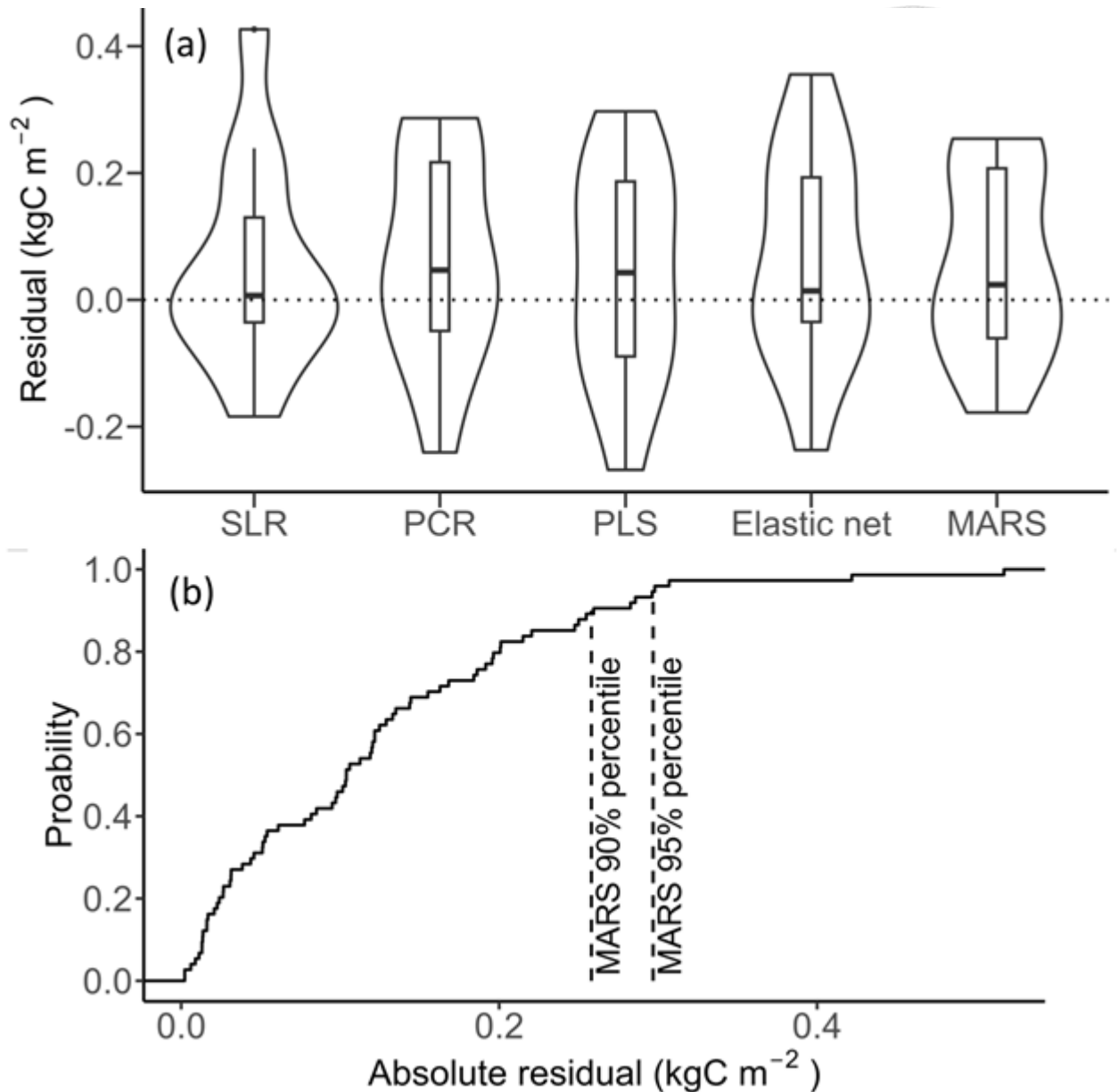
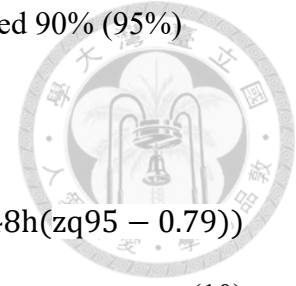


**Fig. 5.** (a) Distributions and statistics of residuals of the test data from the best-tuned models (see 2.5 for the acronyms). (b) Empirical cumulative probability distribution of the absolute value of residuals from MARS.

Residuals of MARS (eq. 10) using test data were bounded within  $-0.18$  and  $0.25$   $\text{kg C m}^{-2}$  (Fig. 5a), the shortest interval among models. We then used the best-tuned hyperparameter of MARS to fit the entire dataset and calculated the empirical cumulative probability function on the absolute value of residuals. The MARS

empirical cumulative probability rose quickly (Fig. 5b) and contained 90% (95%) absolute residuals within  $0.26 \text{ kgC m}^{-2}$  ( $0.30 \text{ kgC m}^{-2}$ ).



$$\widehat{AGC} = 0.53 - 0.49h(z_{\max} - 1.48) + 0.77h(z_{q65} - 0.97) + 0.48h(z_{q95} - 0.79) \quad (10)$$

**Table 3.** Coefficients and adjusted  $R^2$  values of standardized multiple linear regressions of using  $z_{\max}$ ,  $z_{q95}$ , and  $z_{q65}$  to model canopy metrics (see Fig. 6d for an example).

Canopy metric	$z_{\max}$	$z_{q95}$	$z_{q65}$	$R_{\text{adj}}^2$
entropy <sub>sH</sub>	-1.30 <sup>***</sup>	0.71	0.56 <sup>**</sup>	0.27 <sup>***</sup>
vp	-1.20 <sup>***</sup>	0.73 <sup>*</sup>	0.90 <sup>**</sup>	0.53 <sup>***</sup>
Rumple index	0.54 <sup>*</sup>	0.28	-0.01	0.53 <sup>***</sup>

<sup>\*\*\*</sup>  $p < 0.001$ , <sup>\*\*</sup>  $p < 0.01$ , <sup>\*</sup>  $p < 0.05$

MARS showed that AGC was mainly influenced by  $z_{\max}$ ,  $z_{q95}$ , and  $z_{q65}$  (eq. 10). The variable importance score of  $z_{q65}$  was three times higher than that of  $z_{\max}$  and  $z_{q95}$ , of which the scores were identical (data not shown). Surprisingly, the three canopy structural metrics (entropy<sub>sH</sub>, vp and the Rumple index) were not included in MARS, which may be explained by other MARS predictors by referring to standardized multiple linear regression (Table 3). Using vp as an example, we found a significant relationship (slope = 1,  $R_{\text{adj}}^2 = 0.53$ ) between observed and MARS predicted vp with  $z_{\max}$ ,  $z_{q95}$ , and  $z_{q65}$  (Fig. 6d), despite weak individual linear relationships (Fig. 6a-c). The correlation between 64 lidar metrics showed that 1301 pairs (65% of total pairs) of variables were correlated ( $p < 0.05$ ).

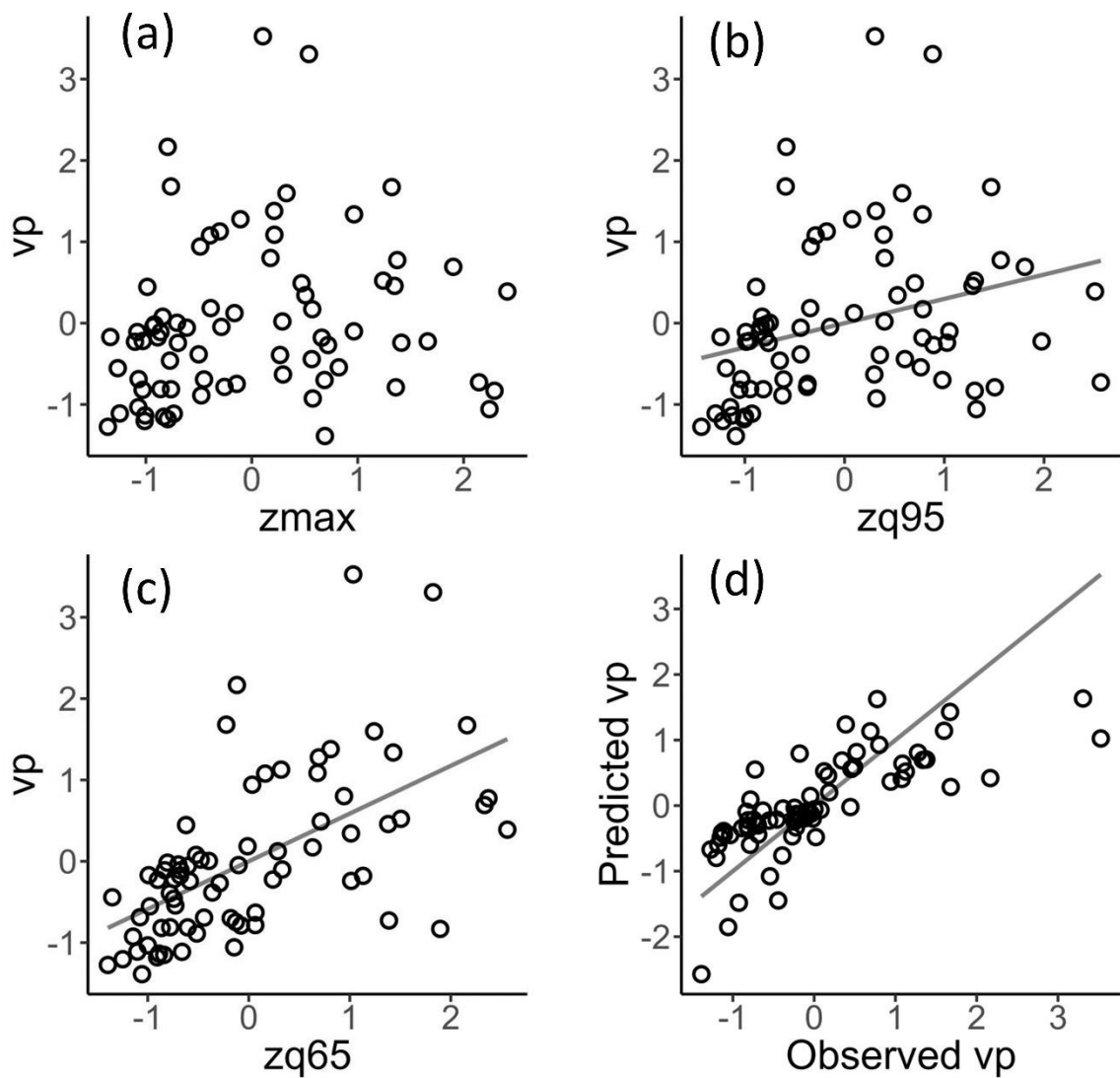


**Fig. 6.** Linear relationships of vp and three salient predictors of MARS, (a) zmax (b) zq95 and (c) zq65. (d) Observed vp and predicted vp from zmax, zq95, and zq65. Gray lines indicate statistically significant ( $p < 0.05$ ).

### 3.3. AGC density mapping

The dwarf bamboo AGC density map and variation (sd) derived using MARS (Milborrow, 2021) showed that open dwarf bamboo was mainly distributed on the south-facing slope and patchily scattered on the north-facing slope (Fig. 7). We found that the AGC density was higher in the area where valleys met the ridge. We also

observed that the carbon density was lower in the flatter areas or on both sides of the ridge. Our preliminary visual assessment indicates that the spatial variation might be related to the local topographic characteristics.

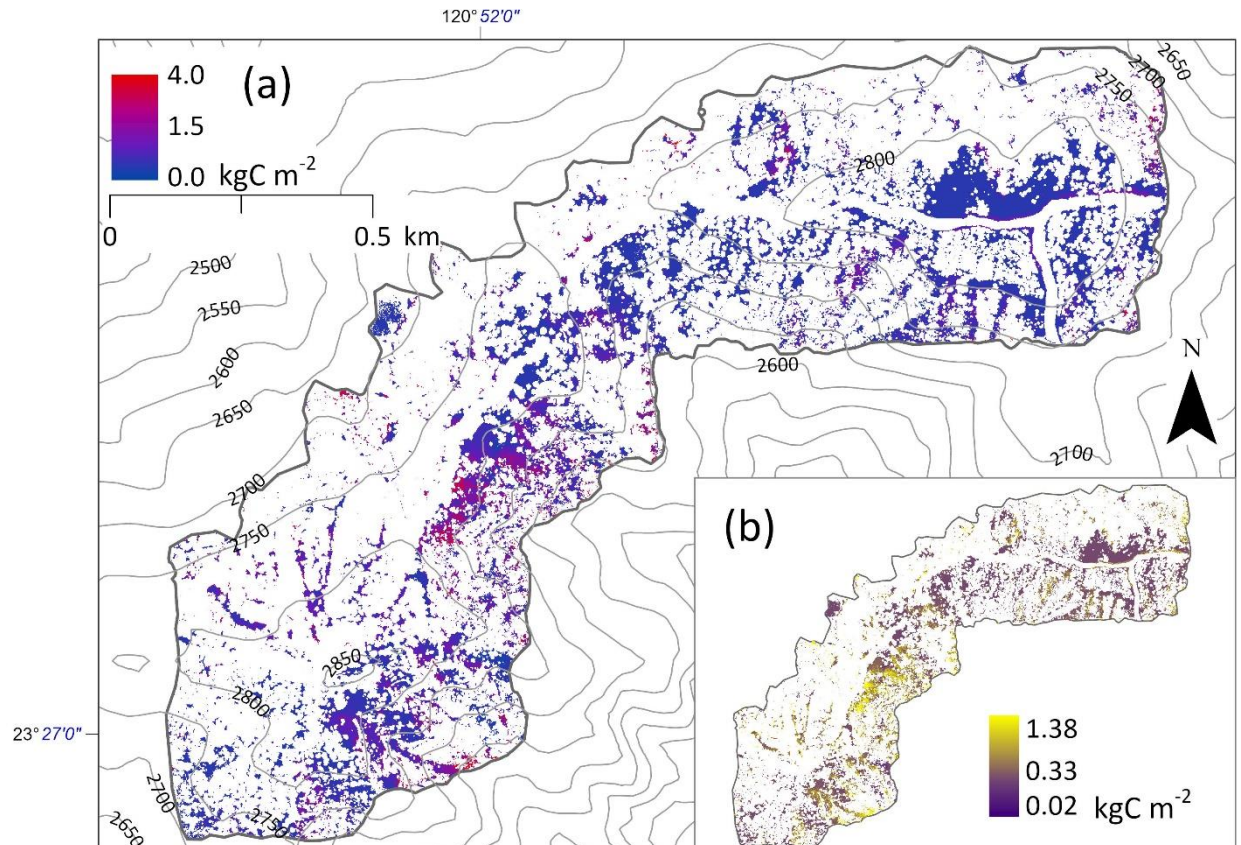
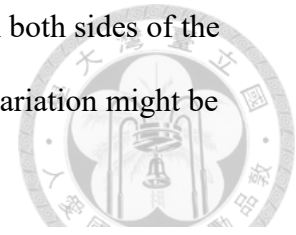


**Fig. 7.** (a) Modeled dwarf bamboo AGC density and (b) standard deviation maps of the study site using MARS. Gray lines are elevation contour lines (unit: m), and the black outline is the boundary of the study region.

## 4. Discussion

### 4.1. AGC density modeling

In this study, we followed a standard UAV lidar data acquisition procedure, including low and fixed flight height, proper side overlap, and low speed, ensuring accurate and dense point cloud data. The generated ground point elevations had an

RMSE < 1.5 cm when compared to ground control points. Abundant lidar returns and precise field sampling provided detailed canopy information for modeling, with the near canopy bottom metric being a significant predictor of dwarf bamboo AGC density. These acquisition practices support the reliability of our approach. For others such as large-sized bamboo species, adjusting field plot size may be necessary.

Spaceborne lidar systems such as the Global Ecosystem Dynamics Investigation (GEDI) and terrestrial laser scanning (TLS) may not be suitable for our case. The footprint of GEDI is 25 m, and its along-track and cross-track spacing is 60 m and 600 m, respectively (Dubayah et al., 2020). These coarse lidar returns do not align with our field plot size and the desired spatial resolution for the task. Additionally, the accuracy of GEDI height data is > 1 m (Adam et al., 2020), making it inadequate for differentiating the canopy of dwarf bamboo. On the other hand, the TLS approach may not be appropriate due to the dense bamboo canopies and rugged mountain terrain (Fig. 1c).

This study demonstrates that UAV-lidar can precisely acquire high density point-cloud data over a mountain landscape and applicable for dwarf bamboo AGC density modeling. We employed linear models to investigate the relationship between the AGC density and UAV-lidar derived metrics, achieving RMSEs  $\leq 0.17 \text{ kgC m}^{-2}$  for both the training and test data (Table 2). The results indicated that elastic net and PCR performed slightly poorer, which may be related to exploiting many more predictors in the training data. In contrast, SLR, PLS, and MARS were relatively more robust, with the exception of SLR, which produced an outlier on test data (Fig. 5a).

According to our comprehensive analysis (Table 2), we conclude that the performance of MARS is superior to that of the other models. Residuals of MARS were also

concentrated the most (Fig. 5), indicating the robustness of the model. MARS allows each predictor to be divided into intervals with the corresponding breakpoints, capturing their unique contributions to AGC density with specific basis functions. This localized approach differs from other linear models, which rely on a single global trend, and may be feasible for delineating the unique structure of bamboo vegetation. MARS also indicated the non-linear nature of AGC density and percentile basis functions. Similar studies have specified model forms by allometric or power law functions that can be extended to model AGC (Asner & Mascaro, 2014; Ferraz et al., 2018; Xu et al., 2017), yet we showed that piecewise linear functions (basis functions) of lidar percentiles would be able to present the non-linearity of AGC density without prior knowledge of the exact form of the non-linear function.

#### 4.2. Salient UAV-lidar metrics for dwarf bamboo AGC mapping

The regression model MARS (eq. 10) selected  $z_{max}$ ,  $zq95$  and  $zq65$  as salient predictors for AGC density. Surprisingly, given the canopy structural metrics  $entropy_{SH}$  (entropy of dwarf bamboo in terms of scaled version of vertical profile),  $vp$  (volumetric percentage of returns, eqs. 2 and 3), and the Rumple index (top surface roughness to reflect compactness of bamboo culms), we found that  $vp$  can be explained by  $z_{max}$ ,  $zq95$ , and  $zq65$  (Table 3 and Fig. 6d), and  $entropy_{SH}$  and the Rumple index can also be explained by  $z_{max}$  or  $zq65$ , suggesting that the inherited multicollinearity between structural metrics and height percentiles excludes these canopy metrics from MARS even in forms of basis functions. The excursion means that these height percentiles can directly represent information on vegetation without canopy profiles.

Applications of UAV or manned airborne lidar on bamboo, forest, shrubs, or

grassland also favor percentiles in top canopy layers as main predictors for biomass estimation (Cao et al., 2019; d'Oliveira et al., 2020; da Costa et al., 2021; Wang et al., 2017; Zhao et al., 2012). In this study, we observed that zq65 is the most significant lidar metric, which has not been reported by previous studies. zq65 is the height of the top of the 13<sup>th</sup> layer, and vp is the percentage of lidar returns between the 19<sup>th</sup> and 13<sup>th</sup> layers, suggesting that zq65 represents the information near the bottom of the canopy that contributes to AGC density prediction. This also showed that conventional modeling approaches using top percentiles or gridded canopy height models might overlook the potentially important percentiles near the bottom of the canopy.

#### 4.3. Dwarf bamboo AGC density and topography

We applied MARS with UAV-lidar metrics to generate a 1-m AGC density map for open dwarf bamboo. We found that the vegetation is predominantly located on south-facing slopes (Fig. 1a), which is consistent with a previously conducted local field study (Liu, 1963). The spatial coverage also revealed that the open dwarf bamboo AGC density varies with slope steepness. Previous research on the dominance of open dwarf bamboo has focused on factors such as slope aspect, soil water content, soil depth, and exposure to wind (Chen et al., 1992), which showed that body size may also be influenced by phenotypic plasticity due to light exposure during growth (Wu & Kao, 2021). These factors likely contribute to the observed spatial variation in open dwarf bamboo AGC density across different settings. We note that here, we only provide preliminary analysis to highlight the potential for regional dwarf bamboo research with the availability of a high-spatial-resolution AGC map. More comprehensive analyses are required to draw more conclusive interpretations to further investigate the biotic and abiotic factors (topography and/or microclimate) shaping the spatial pattern of dwarf bamboo abundance (e.g., Lai et al. 2021).



## 5. Conclusions

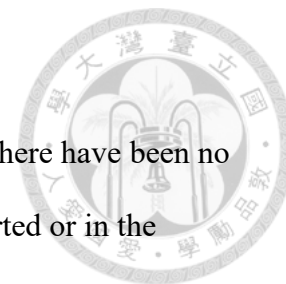
Our study highlights the feasibility of UAV-lidar point-cloud data and field sampling with linear models to generate a 1-m AGC density map. Issues of similar canopy structure among different body sizes due to the rapid growth of bamboo, undulating AGC density arising from the composition of new and old culms, or contrasting spectral reflectance corresponding to similar AGC density can be bypassed using UAV-lidar. Our analysis of dwarf bamboo AGC density assessment shows that MARS with lidar height metrics ( $z_{\max}$  [maximum height of point cloud],  $z_{q95}$  and  $z_{q65}$  [95<sup>th</sup> and 65<sup>th</sup> percentiles of height distribution, respectively]), particularly  $z_{q65}$ , may precisely model dwarf bamboo AGC density. The regional estimation of the dwarf bamboo AGC map may facilitate comprehensive analysis of spatial patterns, which could shed some light on the factors driving carbon-content variation in subalpine vegetation.

## Acknowledgments

We appreciate the field assistance provided by Chih-I Lin and Cheng-Han Lu (Kang Ying Enterprise Ltd.), Wen-Tiao Liao, and Ciou-Hui Wu. This work was supported by the National Science and Technology Council (111-2121-M-002-001-), Taiwan Forestry Research Institute (111AS-7.1.2-FI-G1), National Taiwan University (NTU-107L9010) and the Research Center for Future Earth, the Featured Areas Research Center Program, the Higher Education Sprout Project, and the Ministry of Education (MOE) in Taiwan.

## **Declaration of interest statement**

The corresponding author confirms on behalf of all authors that there have been no involvements that might raise the question of bias in the work reported or in the conclusions, implications, or opinions stated.



## **Author contributions statement**

Hsiao-Lung Pan: Formal analysis, Data curation, Resources, Conceptualization, Methodology, Investigation, Resources, Data curation, Writing - original draft, Visualization, Project administration, Funding acquisition

Chu-Mei Huang: Data curation

Cho-ying Huang: Conceptualization, Methodology, Investigation, Resources, Data curation, Writing - original draft, Writing - review & editing, Visualization, Supervision, Funding acquisition


## **Data availability statement**

The data that support the findings of this study will be openly available in Zenodo upon the acceptance of the manuscript.

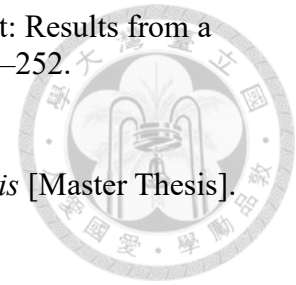
## **Declaration of Generative AI and AI-assisted technologies in the writing process**

During the preparation of this work the authors used ChatGPT-4 in order to enhance the flow of the manuscript. After using this tool/service, the authors reviewed and edited the content as needed and take full responsibility for the content of the publication.

## References

- 
- Adam, M., Urbazaev, M., Dubois, C., & Schmillius, C. (2020). Accuracy Assessment of GEDI Terrain Elevation and Canopy Height Estimates in European Temperate Forests: Influence of Environmental and Acquisition Parameters. *Remote Sensing*, 12(23), Article 23. <https://doi.org/10.3390/rs12233948>
- Akinlabi, E. T., Anane-Fenin, K., & Akwada, D. R. (2017). Bamboo as Fuel. In E. T. Akinlabi, K. Anane-Fenin, & D. R. Akwada (Eds.), *Bamboo: The Multipurpose Plant* (pp. 149–178). Springer International Publishing. [https://doi.org/10.1007/978-3-319-56808-9\\_4](https://doi.org/10.1007/978-3-319-56808-9_4)
- Asner, G. P., Flint Hughes, R., Varga, T. A., Knapp, D. E., & Kennedy-Bowdoin, T. (2009). Environmental and Biotic Controls over Aboveground Biomass Throughout a Tropical Rain Forest. *Ecosystems*, 12(2), 261–278. <https://doi.org/10.1007/s10021-008-9221-5>
- Asner, G. P., & Mascaro, J. (2014). Mapping tropical forest carbon: Calibrating plot estimates to a simple LiDAR metric. *Remote Sensing of Environment*, 140, 614–624. <https://doi.org/10.1016/j.rse.2013.09.023>
- Beland, M., Parker, G., Sparrow, B., Harding, D., Chasmer, L., Phinn, S., Antonarakis, A., & Strahler, A. (2019). On promoting the use of lidar systems in forest ecosystem research. *Forest Ecology and Management*, 450, 117484. <https://doi.org/10.1016/j.foreco.2019.117484>
- Bystriakova, N., Kapos, V., Lysenko, I., & Stapleton, C. M. A. (2003). Distribution and conservation status of forest bamboo biodiversity in the Asia-Pacific Region. *Biodiversity & Conservation*, 12(9), 1833–1841. <https://doi.org/10.1023/A:1024139813651>
- Bystriakova, N., Kapos, V., Lysenko, I., UNEP World Conservation Monitoring Centre, & International Network for Bamboo and Rattan. (2004). *Bamboo biodiversity: Africa, Madagascar and the Americas*. Cambridge, United Kingdom : UNEP-WCMC ; Beijing : INBAR. <http://archive.org/details/bamboobiodiversi04byst>
- Cao, L., Coops, N. C., Sun, Y., Ruan, H., Wang, G., Dai, J., & She, G. (2019). Estimating canopy structure and biomass in bamboo forests using airborne LiDAR data. *ISPRS Journal of Photogrammetry and Remote Sensing*, 148, 114–129. <https://doi.org/10.1016/j.isprsjprs.2018.12.006>
- Chang, M.-H. (1981). *Ecology and control of Yushan cane* [Master Thesis]. National Taiwan University.
- Chave, J., Condit, R., Lao, S., Caspersen, J. P., Foster, R. B., & Hubbell, S. P. (2003).

Spatial and temporal variation of biomass in a tropical forest: Results from a large census plot in Panama. *Journal of Ecology*, 91(2), 240–252. <https://doi.org/10.1046/j.1365-2745.2003.00757.x>



Chen, C.-F. (1983). *Resource allocation of Yushania niitakayamensis* [Master Thesis]. National Taiwan University.

Chen, Y., JY, L., & CK, W. (1992). Ecological research on high-mountain vegetation in Taiwan (II)—The variation in growth form in Yushan cane. *Yushania*, 6, 117–143.

Chen, Y., Li, L., Lu, D., & Li, D. (2019). Exploring Bamboo Forest Aboveground Biomass Estimation Using Sentinel-2 Data. *Remote Sensing*, 11(1), Article 1. <https://doi.org/10.3390/rs11010007>

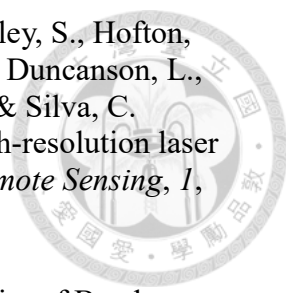
Chiang, W., & Chang, S. (2010). The Analyses of Mt. Lulin Background Station Monitoring Data from 2006 to 2009. In *Bulletin of Environmental Monitoring and Information Techniques* (Vol. 5, pp. 20–34). Department of Environmental Monitoring and Information management, Environmental Protection Administration, Executive Yuan, R.O.C (Taiwan). <https://sites.google.com/site/twepal01/zhai-yao5-2>

d'Oliveira, M., Broadbent, E., Oliveira, L., Almeida, D., Papa, D., Ferreira, M., Zambrano, A., Silva, C., Avino, F., Prata, G., Mello, R., Figueiredo, E., Jorge, L., Junior, L., Albuquerque, R., Brancalion, P., Wilkinson, B., & Oliveira-da-Costa, M. (2020). Aboveground Biomass Estimation in Amazonian Tropical Forests: A Comparison of Aircraft- and GatorEye UAV-borne LiDAR Data in the Chico Mendes Extractive Reserve in Acre, Brazil. *Remote Sensing*, 12(11), 1754. <https://doi.org/10.3390/rs12111754>

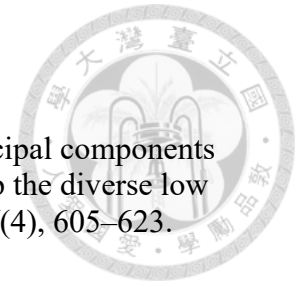
da Costa, M. B. T., Silva, C. A., Broadbent, E. N., Leite, R. V., Mohan, M., Liesenberg, V., Stoddart, J., do Amaral, C. H., de Almeida, D. R. A., da Silva, A. L., Ré Y. Goya, L. R., Cordeiro, V. A., Rex, F., Hirsch, A., Marcatti, G. E., Cardil, A., de Mendonça, B. A. F., Hamamura, C., Corte, A. P. D., ... Klauberg, C. (2021). Beyond trees: Mapping total aboveground biomass density in the Brazilian savanna using high-density UAV-lidar data. *Forest Ecology and Management*, 491, 119155. <https://doi.org/10.1016/j.foreco.2021.119155>

Dayal, Bhupinder. S., & MacGregor, J. F. (1997). Improved PLS algorithms. *Journal of Chemometrics*, 11(1), 73–85. [https://doi.org/10.1002/\(SICI\)1099-128X\(199701\)11:1<73::AID-CEM435>3.0.CO;2-#](https://doi.org/10.1002/(SICI)1099-128X(199701)11:1<73::AID-CEM435>3.0.CO;2-#)

Dhaliwal, G. S., Gupta, N., Kukal, S. S., & Meetpal-Singh. (2014). Standardization of Automated Vario EL III CHNS Analyzer for Total Carbon and Nitrogen Determination in Plants. *Communications in Soil Science and Plant Analysis*, 45(10), 1316–1324. <https://doi.org/10.1080/00103624.2013.875197>

- 
- Dubayah, R., Blair, J. B., Goetz, S., Fatoyinbo, L., Hansen, M., Healey, S., Hofton, M., Hurtt, G., Kellner, J., Luthcke, S., Armston, J., Tang, H., Duncanson, L., Hancock, S., Jantz, P., Marselis, S., Patterson, P. L., Qi, W., & Silva, C. (2020). The Global Ecosystem Dynamics Investigation: High-resolution laser ranging of the Earth's forests and topography. *Science of Remote Sensing, 1*, 100002. <https://doi.org/10.1016/j.srs.2020.100002>
- Engler, B., Schoenherr, S., Zhong, Z., & Becker, G. (2012). Suitability of Bamboo as an Energy Resource: Analysis of Bamboo Combustion Values Dependent on the Culm's Age. *International Journal of Forest Engineering, 23*(2), 114–121. <https://doi.org/10.1080/14942119.2012.10739967>
- Ferraz, A., Saatchi, S., Xu, L., Hagen, S., Chave, J., Yu, Y., Meyer, V., Garcia, M., Silva, C., Roswintiar, O., Samboko, A., Sist, P., Walker, S., Pearson, T. R. H., Wijaya, A., Sullivan, F. B., Rutishauser, E., Hoekman, D., & Ganguly, S. (2018). Carbon storage potential in degraded forests of Kalimantan, Indonesia. *Environmental Research Letters, 13*(9), 095001. <https://doi.org/10.1088/1748-9326/aad782>
- Friedman, J. H., Hastie, T., & Tibshirani, R. (2010). Regularization Paths for Generalized Linear Models via Coordinate Descent. *Journal of Statistical Software, 33*, 1–22. <https://doi.org/10.18637/jss.v033.i01>
- Greenwell, B., Boehmke, B., & Gray, B. (2020). *vip: Variable Importance Plots (0.3.2)*. <https://CRAN.R-project.org/package=vip>
- Han, L., Yang, G., Dai, H., Xu, B., Yang, H., Feng, H., Li, Z., & Yang, X. (2019). Modeling maize above-ground biomass based on machine learning approaches using UAV remote-sensing data. *Plant Methods, 15*(1), 10. <https://doi.org/10.1186/s13007-019-0394-z>
- Harrell, F. E. (2015). Multivariable Modeling Strategies. In Jr. Harrell Frank E. (Ed.), *Regression Modeling Strategies: With Applications to Linear Models, Logistic and Ordinal Regression, and Survival Analysis* (pp. 63–102). Springer International Publishing. [https://doi.org/10.1007/978-3-319-19425-7\\_4](https://doi.org/10.1007/978-3-319-19425-7_4)
- Hastie, T., Qian, J., & Tay, K. (2021, November 1). *An Introduction to 'glmnet'*. An Introduction to Glmnet. <https://glmnet.stanford.edu/articles/glmnet.html#ref-glmnet>
- Hastie, T., Tibshirani, R., & Friedman, J. (2009). Additive Models, Trees, and Related Methods. In T. Hastie, R. Tibshirani, & J. Friedman (Eds.), *The Elements of Statistical Learning: Data Mining, Inference, and Prediction* (pp. 295–336). Springer. [https://doi.org/10.1007/978-0-387-84858-7\\_9](https://doi.org/10.1007/978-0-387-84858-7_9)
- Huang, C., Liu, H.-C., Hu, K.-T., Chung, C.-H., & Wang, J. (2023). Variation of seasonal litterfall in subtropical montane cloud forests to typhoon severity and

environmental factors. *Biotropica*, 55(1), 132–144.  
<https://doi.org/10.1111/btp.13166>



- Huang, C., Wei, H.-L., Rau, J.-Y., & Jhan, J.-P. (2019). Use of principal components of UAV-acquired narrow-band multispectral imagery to map the diverse low stature vegetation fAPAR. *GIScience & Remote Sensing*, 56(4), 605–623.  
<https://doi.org/10.1080/15481603.2018.1550873>
- James, G., Witten, D., Hastie, T., & Tibshirani, R. (2021). *An Introduction to Statistical Learning: With Applications in R (Hardcover)* (Second). Springer.  
<https://www.statlearning.com/>
- Karna, Y. K., Penman, T. D., Aponte, C., Hinko-Najera, N., & Bennett, L. T. (2020). Persistent changes in the horizontal and vertical canopy structure of fire-tolerant forests after severe fire as quantified using multi-temporal airborne lidar data. *Forest Ecology and Management*, 472, 118255.  
<https://doi.org/10.1016/j.foreco.2020.118255>
- Kudo, G., Amagai, Y., Hoshino, B., & Kaneko, M. (2011). Invasion of dwarf bamboo into alpine snow-meadows in northern Japan: Pattern of expansion and impact on species diversity. *Ecology and Evolution*, 1(1), 85–96.  
<https://doi.org/10.1002/ece3.9>
- Kuhn, M. (2019). *5 Model Training and Tuning | The caret Package*.  
<http://topepo.github.io/caret/model-training-and-tuning.html#custom>
- Kuhn, M., Wing, J., Weston, S., Williams, A., Keefer, C., Engelhardt, A., Cooper, T., Mayer, Z., Kenkel, B., R Core Team, Benesty, M., Lescarbeau, R., Ziem, A., Scrucca, L., Tang, Y., Candan, C., & Hunt, T. (2022). *caret: Classification and Regression Training* (6.0-93). <https://CRAN.R-project.org/package=caret>
- Kumar, D., & Mandal, A. (2022). Review on manufacturing and fundamental aspects of laminated bamboo products for structural applications. *Construction and Building Materials*, 348, 128691.  
<https://doi.org/10.1016/j.conbuildmat.2022.128691>
- Lai, G.-Y., Liu, H.-C., Chung, C.-H., Wang, C.-K., & Huang, C. (2021). Lidar-derived environmental drivers of epiphytic bryophyte biomass in tropical montane cloud forests. *Remote Sensing of Environment*, 253, 112166.  
<https://doi.org/10.1016/j.rse.2020.112166>
- Li, Y., Han, N., Li, X., Du, H., Mao, F., Cui, L., Liu, T., & Xing, L. (2018). Spatiotemporal Estimation of Bamboo Forest Aboveground Carbon Storage Based on Landsat Data in Zhejiang, China. *Remote Sensing*, 10(6), Article 6.  
<https://doi.org/10.3390/rs10060898>
- Liu, Z., Fei, B., Jiang, Z., Cai, Z., & Liu, X. (2014). Important properties of bamboo

pellets to be used as commercial solid fuel in China. *Wood Science and Technology*, 48(5), 903–917. <https://doi.org/10.1007/s00226-014-0648-x>

- Lobovikov, M., Paudel, S., Piazza, M., Hong Ren, Junqi Wu, & Forestry Economics and Policy Division. (2007). *World bamboo resources: A thematic study prepared in the framework of the Global Forest Resources Assessment 2005*. FAO. <https://www.fao.org/publications/card/en/c/116d1258-a4cb-5527-926b-8b4911f44781/>
- Lobovikov, M., Schoene, D., & Yping, L. (2012). Bamboo in climate change and rural livelihoods. *Mitigation and Adaptation Strategies for Global Change*, 17(3), 261–276. <https://doi.org/10.1007/s11027-011-9324-8>
- McClure, F. A. (2013). The Bamboos: A Fresh Perspective. In *The Bamboos*. Harvard University Press. <https://doi.org/10.4159/harvard.9780674428713>
- Milborrow, S. (2021). *earth: Multivariate Adaptive Regression Splines (5.3.1)*. <https://CRAN.R-project.org/package=earth>
- Ministry of Digital Affairs, Taiwan. (n.d.). *Taiwan 20M DEM*. Government Open Data. Retrieved June 8, 2023, from <https://data.gov.tw/dataset/35430>
- Patil, P., Singh, S., & Dadhwal, V. K. (2012). Above Ground Forest Phytomass Assessment in Southern Gujarat. *Journal of the Indian Society of Remote Sensing*, 40(1), 37–46. <https://doi.org/10.1007/s12524-011-0121-3>
- Réjou-Méchain, M., Tanguy, A., Piponiot, C., Chave, J., & Hérault, B. (2017). biomass: An r package for estimating above-ground biomass and its uncertainty in tropical forests. *Methods in Ecology and Evolution*, 8(9), 1163–1167. <https://doi.org/10.1111/2041-210X.12753>
- Roussel, J.-R., Auty, D., Coops, N. C., Tompalski, P., Goodbody, T. R. H., Meador, A. S., Bourdon, J.-F., de Boissieu, F., & Achim, A. (2020). lidR: An R package for analysis of Airborne Laser Scanning (ALS) data. *Remote Sensing of Environment*, 251, 112061. <https://doi.org/10.1016/j.rse.2020.112061>
- Safford, H. D. (2001). Brazilian Páramos. III. Patterns and Rates of Postfire Regeneration in the Campos de Altitude1. *BIOTROPICA*, 33(2), 282–302. [https://doi.org/10.1646/0006-3606\(2001\)033\[0282:BPRIPA\]2.0.CO;2](https://doi.org/10.1646/0006-3606(2001)033[0282:BPRIPA]2.0.CO;2)
- Scurlock, J. M. O., Dayton, D. C., & Hames, B. (2000). Bamboo: An overlooked biomass resource? *Biomass and Bioenergy*, 19(4), 229–244. [https://doi.org/10.1016/S0961-9534\(00\)00038-6](https://doi.org/10.1016/S0961-9534(00)00038-6)
- Takano, K. T., Hibino, K., Numata, A., Oguro, M., Aiba, M., Shiogama, H., Takayabu, I., & Nakashizuka, T. (2017). Detecting latitudinal and altitudinal expansion of invasive bamboo *Phyllostachys edulis* and *Phyllostachys bambusoides*

(Poaceae) in Japan to project potential habitats under 1.5°C–4.0°C global warming. *Ecology and Evolution*, 7(23), 9848–9859.  
<https://doi.org/10.1002/ece3.3471>



- Liu, T. (1963). *Ecological study on the high mountain meadow of Mt. Hsiao-Hsueh*. Taiwan Forestry Research Institute.
- Venkatappa, M., Anantsuksomsri, S., Castillo, J. A., Smith, B., & Sasaki, N. (2020). Mapping the Natural Distribution of Bamboo and Related Carbon Stocks in the Tropics Using Google Earth Engine, Phenological Behavior, Landsat 8, and Sentinel-2. *Remote Sensing*, 12(18), Article 18.  
<https://doi.org/10.3390/rs12183109>
- Vogtländer, J., van der Lugt, P., & Brezet, H. (2010). The sustainability of bamboo products for local and Western European applications. LCAs and land-use. *Journal of Cleaner Production*, 18(13), 1260–1269.  
<https://doi.org/10.1016/j.jclepro.2010.04.015>
- Wang, D., Wan, B., Qiu, P., Zuo, Z., Wang, R., & Wu, X. (2019). Mapping Height and Aboveground Biomass of Mangrove Forests on Hainan Island Using UAV-LiDAR Sampling. *Remote Sensing*, 11(18), Article 18.  
<https://doi.org/10.3390/rs11182156>
- Wang, D., Xin, X., Shao, Q., Brolly, M., Zhu, Z., & Chen, J. (2017). Modeling Aboveground Biomass in Hulunber Grassland Ecosystem by Using Unmanned Aerial Vehicle Discrete Lidar. *Sensors (Basel, Switzerland)*, 17(1).  
<https://doi.org/10.3390/s17010180>
- Wang, J., Du, H., Li, X., Mao, F., Zhang, M., Liu, E., Ji, J., & Kang, F. (2021). Remote Sensing Estimation of Bamboo Forest Aboveground Biomass Based on Geographically Weighted Regression. *Remote Sensing*, 13(15), Article 15.  
<https://doi.org/10.3390/rs13152962>
- Winkler, D. E., Amagai, Y., Huxman, T. E., Kaneko, M., & Kudo, G. (2016). Seasonal dry-down rates and high stress tolerance promote bamboo invasion above and below treeline. *Plant Ecology*, 217(10), 1219–1234.  
<https://doi.org/10.1007/s11258-016-0649-y>
- Wu, K.-S., & Kao, W.-Y. (2021). Phenotypic plasticity and genetic variation in leaf traits of *Yushania niitakayamensis* (Bambusoideae; Poaceae) in contrasting light environments. *Journal of Plant Research*.  
<https://doi.org/10.1007/s10265-021-01327-y>
- Xu, L., Saatchi, S. S., Shapiro, A., Meyer, V., Ferraz, A., Yang, Y., Bastin, J.-F., Banks, N., Boeckx, P., Verbeeck, H., Lewis, S. L., Muanza, E. T., Bongwele, E., Kayembe, F., Mbenza, D., Kalau, L., Mukendi, F., Ilunga, F., & Ebuta, D. (2017). Spatial Distribution of Carbon Stored in Forests of the Democratic



Republic of Congo. *Scientific Reports*, 7(1), Article 1.  
<https://doi.org/10.1038/s41598-017-15050-z>



- Yuen, J. Q., Fung, T., & Ziegler, A. D. (2017). Carbon stocks in bamboo ecosystems worldwide: Estimates and uncertainties. *Forest Ecology and Management*, 393, 113–138. <https://doi.org/10.1016/j.foreco.2017.01.017>
- Zeng, N., Ren, X., He, H., Zhang, L., Zhao, D., Ge, R., Li, P., & Niu, Z. (2019). Estimating grassland aboveground biomass on the Tibetan Plateau using a random forest algorithm. *Ecological Indicators*, 102, 479–487. <https://doi.org/10.1016/j.ecolind.2019.02.023>
- Zhao, F., Guo, Q., & Kelly, M. (2012). Allometric equation choice impacts lidar-based forest biomass estimates: A case study from the Sierra National Forest, CA. *Agricultural and Forest Meteorology*, 165, 64–72. <https://doi.org/10.1016/j.agrformet.2012.05.019>
- Zhao, X., Guo, Q., Su, Y., & Xue, B. (2016). Improved progressive TIN densification filtering algorithm for airborne LiDAR data in forested areas. *ISPRS Journal of Photogrammetry and Remote Sensing*, 117, 79–91. <https://doi.org/10.1016/j.isprsjprs.2016.03.016>
- Zhao, Y., Liu, X., Wang, Y., Zheng, Z., Zheng, S., Zhao, D., & Bai, Y. (2021). UAV-based individual shrub aboveground biomass estimation calibrated against terrestrial LiDAR in a shrub-encroached grassland. *International Journal of Applied Earth Observation and Geoinformation*, 101, 102358. <https://doi.org/10.1016/j.jag.2021.102358>

**APPENDIX B. Spatial clustering moderates the subalpine dwarf bamboo AGC density on environmental gradients in a tropical island**

*To be submitted to Advances in Bamboo Science*

Hsiao-Lung Pan<sup>a,b</sup>, Cho-ying Huang<sup>a</sup>

<sup>a</sup>Department of Geography, National Taiwan University, Taipei 10617, Taiwan

<sup>b</sup>Technical Service Division, Taiwan Forestry Research Institute, Taipei 10066, Taiwan

Corresponding author: Cho-ying Huang (e-mail: [choying@ntu.edu.tw](mailto:choying@ntu.edu.tw))

Address: 1 Sec. 4, Roosevelt Rd., Taipei, Taiwan 10617



## Abstract

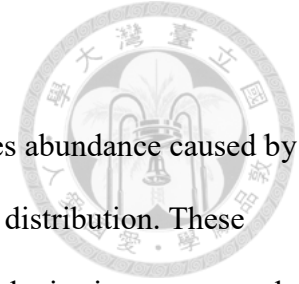


Vegetation is greatly affected by temperatures and rainfall patterns. However, complex terrain and the resulting light, wind, and topographical features influence vegetation aboveground carbon storage (AGC) density variation. Meanwhile, the spatial clustering of high or low AGC density that may affect the relationship between local environmental factors and AGC density is often not included. In this study, we used a 1-meter spatial resolution of AGC density map of subalpine dwarf bamboo, as well as downscaled radiation, wind speed and direction, and micro-topographical features, both of which were previously produced from UAV-lidar point cloud data. Our goal was to understand the influence of the spatial clustering of subalpine dwarf bamboo on AGC variation and explore its differing responses to the factors. We tested the hypotheses that H1: Vegetation spatial clustering better explains the variation of AGC density than environmental factors alone and H2: The various responses of AGC density on environmental gradients are conditioned by the spatial clustering types to understand the contribution of vegetation clustering on AGC variability comparing to environment factors. Our results showed that the spatial clustering of dwarf bamboo significantly improved the estimation of AGC density variation, and the influence of factors on AGC density varies significantly under different clustering types. AGC density in hotspots was influenced by the spring solar irradiation, wind direction, and interaction of wind speed and direction, the slope standard

deviation, and slope influence. At the same time, coldspots had no significant relationship with environmental factors but the clustering. The spatial clustering may be related to the body size and phenotypic plasticity of dwarf bamboo; therefore, we argue that the spatial clustering of dwarf bamboo facilitates effectively utilizing different environmental factors and may be less susceptible to environmental changes.

**Keywords:** aboveground carbon storage, spatial clustering, solar radiation downscaling, wind simulation, UAV-lidar point cloud

## 1. Introduction



Alpine and subalpine ecosystems are subject to changes in species abundance caused by rising temperatures and changing rainfall patterns, which alter their distribution. These changes also impact the amount of carbon stored locally. However, the intricate topography of these regions creates uneven terrain with varying elevations and depressions. This microtopography can cause some areas to receive less solar radiation and experience different wind speeds and directions, resulting in contrasting habitats (Bickford et al., 2011; Marquis et al., 2021). These differences in radiation, temperature, relative humidity, wind speed, and surface drainage due to micro-topographical differences lead to microclimate variations, affecting the vegetation growing in these areas.

The degree to which environmental factors affect plant growth and morphology depends on their magnitudes, gradients, and spatial distributions. Previous studies have found strong correlations between gradients of environmental factors such as slope, aspect, or global sky view factor and local plant communities' diversity and species composition. Due to the influence of solar incident angle and local topographic shading when solar radiation enters a slope, the amount of incoming radiation within a region varies spatially. The red to far-red light ratio (R/FR) affects plants' elongation growth (Panigrahy et al., 2020; Baskin, 2009), and a lower solar incident angle has a smaller R/FR ratio. Therefore, the radiation of lower solar incident angle, which corresponds to the dawn or dusk of a day, during the growing season may also be related to AGC variability. However, if the total daily irradiation is higher, it may create stress and decrease AGC density.

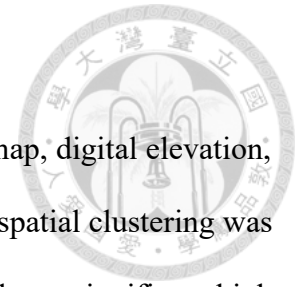
Wind speed also affects plant growth and morphology (Schindler et al., 2012). Low wind speed facilitates photosynthesis and reduces heat accumulation. In contrast, high wind may

cause mechanical damage to the plant body and alter morphology and height (Privé & Allain, 2000), affecting AGC density. Prevailing wind speed and direction can explain differences between habitats and the effect of prevailing wind on vegetation in the same region. Wind field simulations can be used to estimate the local micro-environmental wind speed and direction produced by the prevailing wind after considering the effects of topography. This can be used to model AGC and evaluate the impact of wind on AGC.

Terrain variability contributes to the variation of incident radiation and wind speed. Micro-topographic features such as local slope, aspect, surface roughness, and relative position can affect local interception of moisture, and soil moisture, thus promoting aboveground biomass and AGC. Therefore, incorporating micro-topographic features into studying environmental factors affecting AGC can supplement or replace the effects of soil or surface water that cannot be directly measured or simulated.

Vegetation can also be influenced by vegetation, mainly when plants form closed canopy (Zellweger et al., 2020) or clusters. Scattered plants are more susceptible to environmental changes, but when vegetation establishes and forms clusters, microclimatic differences can occur within or outside the clusters. These differences can create more favorable habitats for plant growth and affect local AGC density. This study suggests that, besides environmental factors, the clustering effect plays a significant role in the spatial variation of AGC in established dominant vegetation. Specifically, the dominant dwarf bamboo vegetation in subalpine regions is more affected by spatial clustering than by environmental factors. Moreover, different types of clustering, such as high or low values or non-significant clustering, can also influence the impact of environmental factors on AGC density. Since dwarf bamboo relies on underground stems for reproduction and above-ground resources to maintain or expand its population, AGC density is influenced by the

population.



This study used a 1-meter above-ground carbon (AGC) density map, digital elevation, and surface models created from UAV lidar point cloud data. AGC spatial clustering was classified into three types: high-value cluster, low-value cluster, and non-significant high or low-value cluster, which represent different types of vegetation clustering. The study also used environmental factors such as incident radiation, wind speed 1 meter above the vegetation, and microtopography features as explanatory variables. We tested two hypotheses: H1 - Vegetation spatial clustering explains more of the variance in AGC density than environmental factors and H2 - The spatial clustering types condition the various responses of AGC density on environmental gradients to understand the contribution of vegetation clustering on AGC variability comparing to environment factors.

## **2. Materials and methods**

### **2.1 Study area**

The study area is located in the Tataka of Yushan National Park, covering an area of approximately 120 ha in subtropical subalpine Taiwan. The terrain mainly comprises two north- and south-facing slopes, with a ridge going from southwest to northeast in between. The elevation in the area ranges from 2600 to 2860 meters a.l.s, with soil thickness of about 20-30 cm (preliminary on-site sampling results). Dominant species include pine trees, hemlocks, and dwarf bamboo, which extensively grows on the south-facing slope or small forms patches on the north-facing slope (Fig. 1).

The Lulin air quality background station (LABS, 23.47°N, 120.87°E, 2862 meters a.s.l.) locates about 500 meters away from the study area and has been observed since 2006. According to the observation of LABS, the study area has an annual average rainfall of

2838 mm, with an average temperature of 11 degrees Celsius, and experiences a humid climate throughout the year. The wet season is April to September, while the frosty months are December to February (Fig. 2).

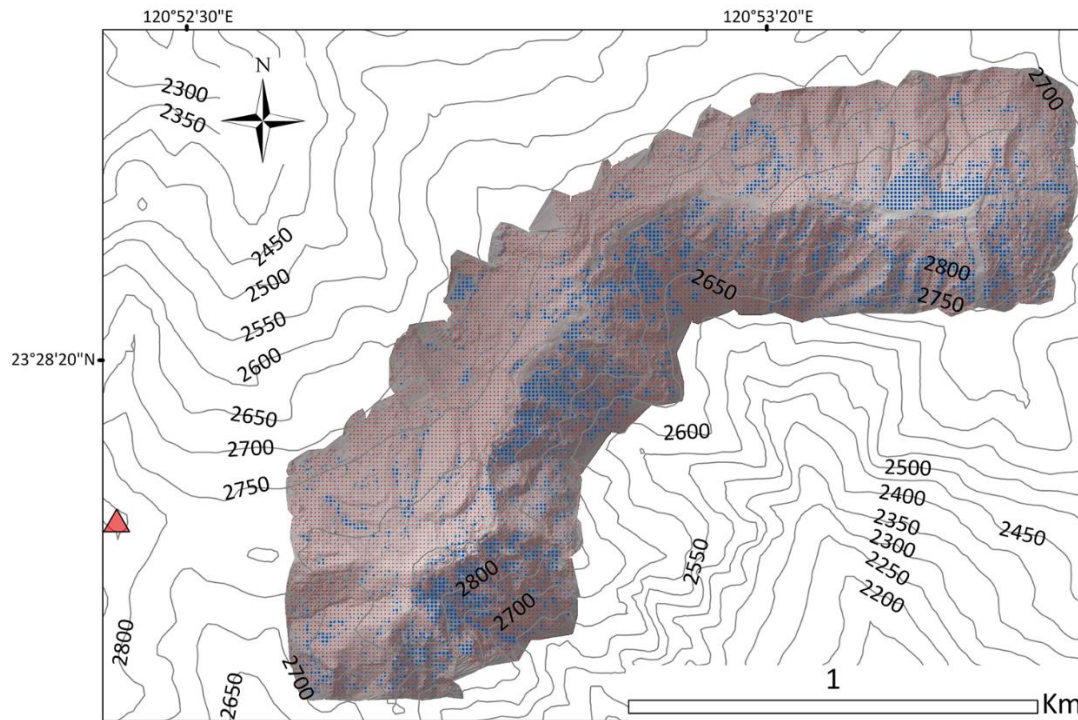


**Fig. 1.** Distribution of dwarf bamboo in Tataka. Shaded relief is generated from the UAV-lidar point cloud (acquisition date:2021/11/27). The blue dot area is dwarf bamboo, and the red dot area is pines and hemlocks. The red triangle is the Lulin air quality background station.



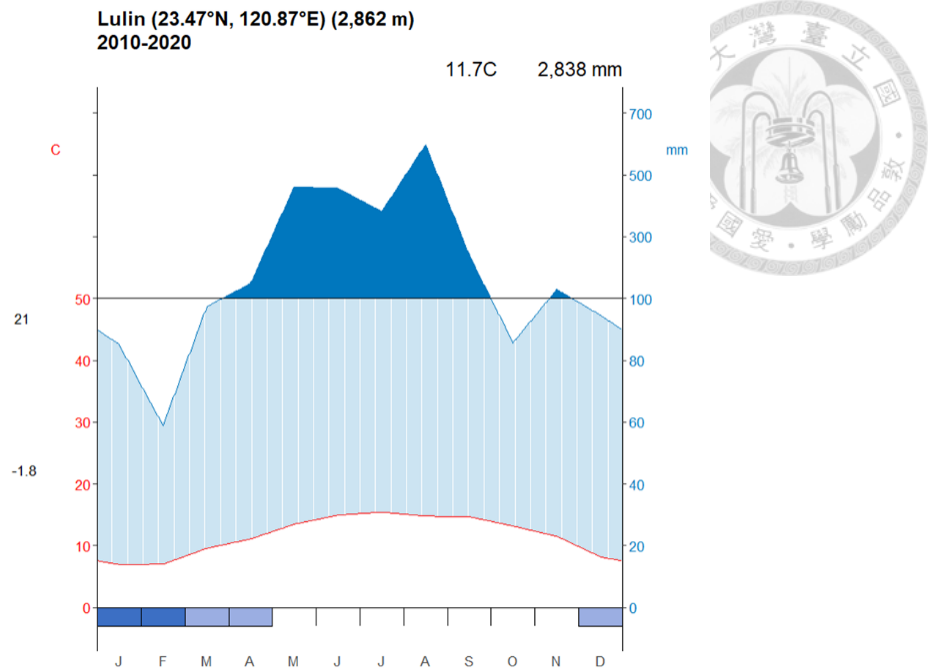


**Fig. 2.** Climate diagram of Tataka based on 2010-2020 observations. The dark blue shade indicates a wet season, while the light blue is humid. The dark blue and light blue bars show the possibility of frost occurrence.

## 2.2 UAV-Lidar derived AGC and digital elevation model

The response variable in this study is the 1-m spatial resolution dwarf bamboo AGC density, sourced from the AGC density map for the Tataka area (Pan et al., 2023) using UAV-lidar point cloud acquired in Nov. 2021. When downscaling the incoming solar radiation or wind speed and direction on a focal surface or extracting the topographical features for the surface, we utilized the point cloud data to generate the digital elevation model (DEM) and digital surface model (DEM) to best correspond to the 1-m AGC density map.

To downscale solar radiation received by each grid in the dwarf bamboo AGC density map, we extracted classification coded as high vegetation (trees) and bare ground, considering the shading from topography and neighboring trees on dwarf bamboo and

accurate inclination angle or horizon angle of slopes for the dwarf bamboo grids, and produced the 1-m DSM. Another 5-m DSM generated from the point cloud of all classifications was used to portray the surface of vegetation and the terrain for downscaling winds in the study area. Lastly, the micro-topographical features were calculated using the 1-m DEM generated from the same point cloud with classification coded as ground points (Fig. 3). All DSMs and DEM were produced using Lidar360 v.5 (Green Valley International, Berkeley, California, USA).

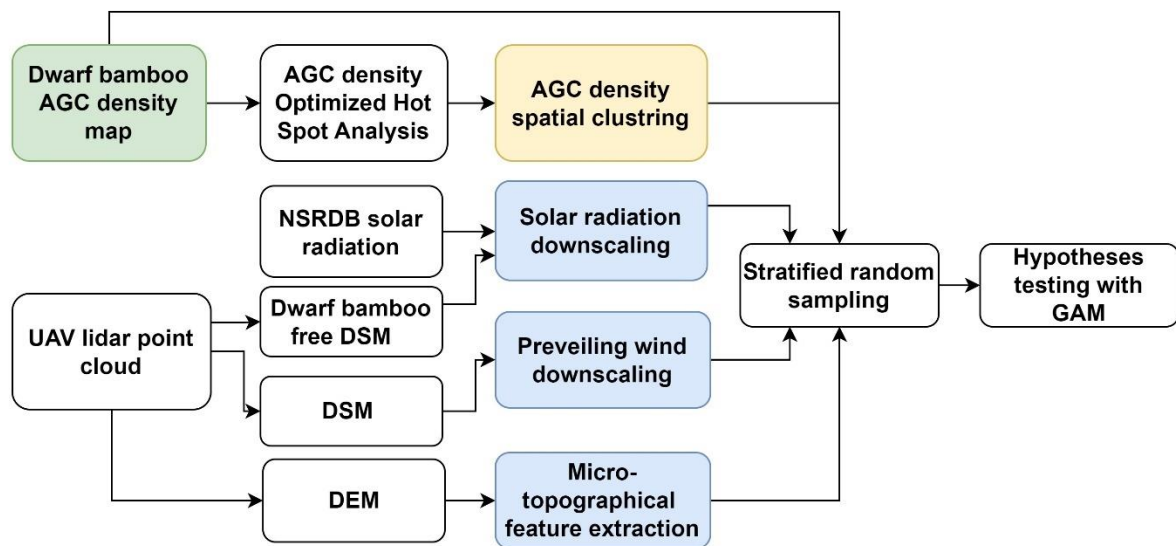


**Fig.3.** The workflow of the study. Pink and blue shade boxes are for generating biotic and abiotic factors, respectively.

### 2.3 Solar radiation downscaling

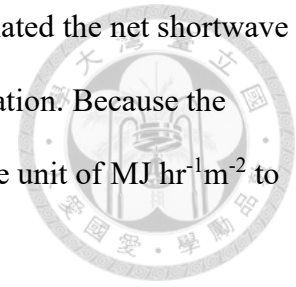
The solar radiation data used in this study was obtained from the National Solar Radiation Database (National Renewable Energy Laboratory, n.d.) for the Asia, Australia, and Pacific regions. The NSRDB provides hourly measurements of global horizontal irradiance (GHI), direct normal irradiance (DNI) and diffuses horizontal irradiance (DHI), and surface albedo at 2 km spatial resolution.

The data used in this study was generated using data from the Himawari satellite and Physical Solar Model (PSM) V3. We divided the study area into 0.01-degree grids and downloaded the solar radiation data for the grid center points using the NSRDB API. We extracted the hourly solar radiation data for March to May during the growing season and generated the gridded data for DHI, DNI, and surface albedo.

We used the generated 1-m DSM and the R package "microclima"(Maclean et al., 2019) to downscale the DHI and DNI raster to a resolution of 1-m. We produced the solar radiation raster for March, April, and May (MAM) from 6 am to 6 pm. Because the solar radiation received by any inclined surface of a grid in a given time is composed of direct, diffuse, and reflected radiation from nearby surfaces, the downscaling procedure involves separating the components' incoming direct and diffuse radiation from the original 2-km resolution solar radiation data and downscaling them to the spatial resolution of the DSM. These components are direct radiation, isotropic and anisotropic diffuse radiation, and reflected radiation from proximity. These are all affected by the topographic shading and proportion of visible sky from an inclined surface in a grid of DSM.

When direct radiation enters the inclined surface, it is shaded by neighboring surfaces if the sun's incident angle is lower than the horizon angle of the surface. On the other hand, when diffuse radiation enters an inclined surface, it is factored by the obstacles in the 360-degree sky view around it. Meanwhile, the anisotropic radiation index calculates the proportion of circumsolar diffuse radiation, and the albedo decides the amount of radiation reflected from the neighboring surface. The "solarindex" function in the microclima package calculates the proportion of direct radiation for a specific time and incident angle to quantify the effect of topographic shadowing on direct radiation and anisotropic diffuse radiation. The "skyviewtopo" function calculates the non-shadowed proportion of the

hemisphere for any focal grid. The "shortwavetopo" function calculated the net shortwave radiation entering the slope and the ratio of anisotropic diffuse radiation. Because the NSRDB radiation data is in units of  $\text{W m}^{-2}$ , we converted data to the unit of  $\text{MJ hr}^{-1}\text{m}^{-2}$  to align with microclima package.



Since an average dwarf bamboo culm have a life span of 5 years(Chen et al., 1992), the UAV-lidar data and AGC density data acquired in 2011, we downscaled solar radiation in 2016-2020 and calculated the daily mean total radiation and low angle radiation (5-6 am and 5-6 pm) for each grid and denoted as *irrad* and *irrad<sub>low</sub>* for the analysis.

#### 2.4 Domain wind average simulation

LABS is located on the top of the ridge extending to the study area and is slightly higher (2862 a.s.l.) than the elevations study area. Therefore, we adopted wind observations in LABS for that in the study area. We used LABS weather observation data to calculate prevailing wind characteristics and simulated wind speed since the lack of wind field data in the study area.

This study used the hourly wind speed and wind direction to estimate seasonal wind speed and direction from 2010 to 2020 and identify the prevailing winds. We also considered diurnal differences and used “openair” package (Carslaw & Ropkins, 2012) in R to create wind roses. We calculated each season's median hourly wind speed and vector mean direction to determine the prevailing wind speed. We also applied the same method to calculate the spring prevailing wind speed and direction of 2016-2020 to match solar radiation data produced in 2.3 and downscale the wind.

WindNinja is a wind diagnostic model developed and sustained by U.S. Forest Service Missoula Fire Sciences Laboratory (Forthofer et al., 2014) and can be used for simulating

mountainous terrain at a fine scale (Wagenbrenner et al., 2016). It offers conservation of mass and conservation of mass and momentum modes to solve the wind field, with the latter providing more accurate results on the lee side at the cost of longer computation time (Missoula Fire Sciences Laboratory, n.d.). The study area is across a central ridge and two major slopes, making the accuracy of the lee-side simulation critical. We used the software to simulate wind fields based on spring prevailing wind direction and speed from 2016-2020. The simulation parameters in WindNinja v3.8 were mesh size 5 m, vegetation trees, wind observation height 10 m, and output height 0.5 m.

## 2.5 Micro-topographical features extraction

This study described micro-topography characteristics using surface roughness since we could not directly measure or simulate the surface precipitation or drainage. The micro-topographic features included standard deviation of slopes in proximity ( $sd_{slope}$ ), slope in degrees, and aspect of a focal grid.  $sd_{slope}$  is the standard deviation of slope within a 5x5 window of the focal grid, and a large  $sd_{slope}$  indicates undulating surfaces in the neighborhood, while small means homogenous surfaces.  $sd_{slope}$  describes the roughness in the adjacent grids. We also included slope and aspect of a focal grid to illustrate the local micro-topography. In this study, the  $sd_{slope}$  were calculated using the "StandardDeviationOfSlope" functions in Whitebox Tools version 2.3.0 (Lindsay, 2014), while slope and aspect were calculated using the "terrain" function in terra package in R.

## 2.6 Spatial clustering of AGC and modeling with microclimatic variables

The spatial clustering of AGC density is the biotic factor in our hypotheses. We converted the AGC density map into polygons of the same size and spatial extent. We then used the "Optimized Hot Spot Analysis" tool in ArcGIS Pro 3.1 (ESRI, Redlands, California, USA) to identify hot spots, cold spots, and non-significant areas of spatial

clustering in the study area. A hotspot indicates a grid with AGC density higher than the mean AGC density is surrounded by grids with similar values. In contrast, a coldspot shows a grid with AGC density lower than the mean AGC density is surrounded by grids of similar values, while the nonsignificant means otherwise. The tool finds the optimized bandwidth of neighbors based on incremental spatial autocorrelation, computes the Getis-Ord  $G_i^*$  statistic (eqs. 1 and 2) of focal grids, and corrects the p-value threshold with the false discovering rate, which deals with issues of multiple testing. We adopted the 99% confidence level to determine whether a focal grid was a hotspot, nonsignificant, or coldspot.

$$G_i^* = \left( \sum_{j=1}^n w_{i,j} x_j - \bar{X} \sum_{j=1}^n w_{i,j} \right) S^{-1} \left( [n-1]^{-1} \left[ n \sum_{j=1}^n w_{i,j}^2 - \left( \sum_{j=1}^n w_{i,j} \right)^2 \right] \right)^{-1/2} \quad (1)$$

$$\text{where } \bar{X} = n^{-1} \left( \sum_{j=1}^n x_j \right) \text{ and } S = \left( n^{-1} \left[ \sum_{j=1}^n x_j^2 \right] - [\bar{X}]^2 \right)^{-1/2} \quad (2)$$

We then randomly sampled 1500 points from each type of spatial clustering and extracted corresponding growing season (MAM) daily solar radiation, low horizontal angle radiation, prevailing wind speed, and micro-topographic features at the sample points. Based on our hypothesis, we established a corresponding generalized additive model (GAM) to test the hypotheses of this study.

GAM represents the response variable as a sum of smooth functions. The advantage of GAM is that the smooth functions explain the non-linear relationship between the response variable and the explanatory variables (James et al., 2021; Wood, 2017), thereby reflecting the non-linear relationship between AGC density and environmental factors. To understand the influence of spatial clustering and environmental factors on AGC density, we propose the following hypotheses: H1- vegetation spatial clustering explains more variance in AGC

density than environmental factors and H2 - the influence of environmental factors on AGC density varies in vegetation spatial clustering. Therefore, we specify the following GAM models to test the effect of spatial clustering, where a smooth function of a covariate  $t$  is in the form of  $s(t)$ , and the error follows a normal distribution with a mean zero and a constant variance. We formulated H1A and H1B to compare the effect of AGC density on model performance with and without spatial clustering type. We also included a smooth function of geographical coordinates,  $s(x, y)$ , to account for the spatial autocorrelation in the sample. Moran's I statistics were calculated for the random sample and residuals of models with bandwidth from 5 to 300 m and step of 5m to assure the residuals are uncorrelated. We also included a tensor interaction term of wind speed and direction ( $ti(speed, dir)$ , see eq.3-5) to model the partial effect of two variables.

$$H1A: AGC = a_1 + s(x, y) + s(irrad) + s(irrad_{low}) + s(speed) + s(dir) + ti(speed, dir) + s(sd_{slope}) + s(slope) + s(aspect) + s(x, y) + \epsilon_1 \quad (3)$$

$$H1B: GC = a_2 + s(x, y) + s(irrad) + s(irrad_{low}) + s(speed) + s(dir) + ti(speed, dir) + s(sd_{slope}) + s(slope) + s(aspect) + s(x, y) + cluster + \epsilon_2 \quad (4)$$

$$H2: AGC = a_3 + s(x, y) + s(irrad, cluster) + s(irrad_{low}, clusetr) + s(speed, cluster) + s(dir, cluster) + ti(speed, dir, cluster) + s(sd_{slope}, cluster) + s(slope, cluster) + s(aspect, cluster) + s(x, y) + cluster + \epsilon_3 \quad (5)$$

We first fitted AGC density with environmental factors derived, including MAM daily solar radiation (*irrad*), daily solar radiation of low incident angle (*irrad<sub>low</sub>*), wind speed (*speed*), wind direction (*dir*), interaction of wind speed and direction, and micro-topographical features *sd<sub>slope</sub>*, *slope*, and *aspect*. (eq. 3). We then added the spatial clustering (*cluster*) in the eq. 3 to measure the effect of hotspot, nonsignificant, and coldspot (eq. 4). Lastly, we incorporated the clustering types into the smooth function to measure the interaction between the explanatory variables and the clustering type and the relationship of

AGC density and the explanatory variables under the clustering types.



### 3. Results

#### 3.1 AGC density spatial clustering

The spatial clustering of AGC density demonstrated that coldspot tends to locate on the northeast side of the study area. At the same time, hotspots are mainly distributed in the middle and the southwest of the study (Fig. 4). Comparing to Fig. 1. We found that coldspot also distributed in both low-slope and high-slope areas, yet hotspots distributed mainly on steep slopes.

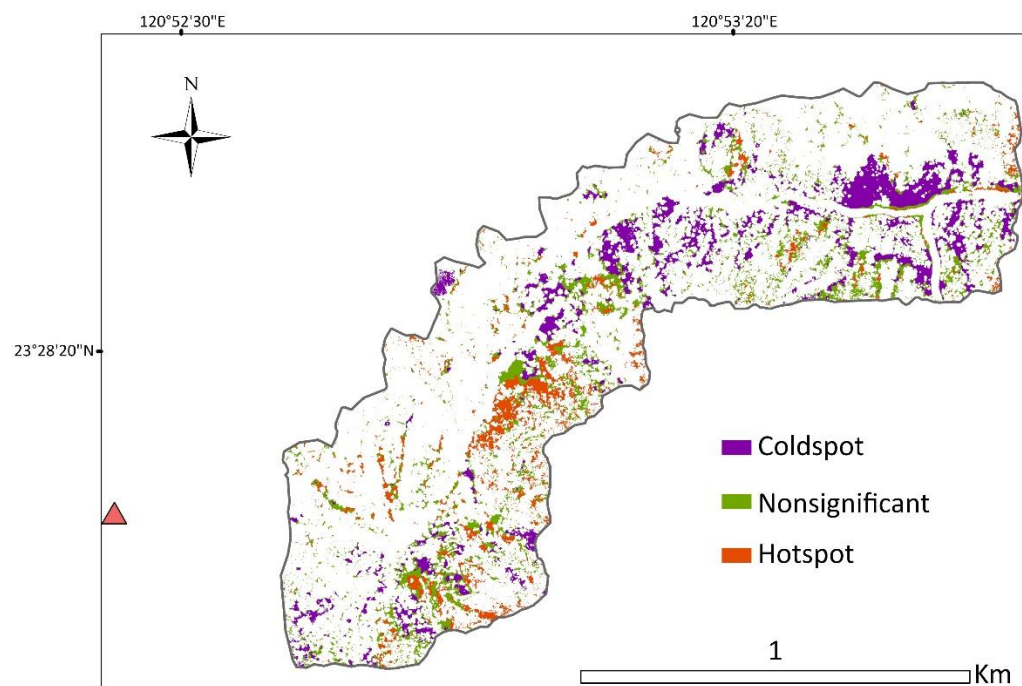


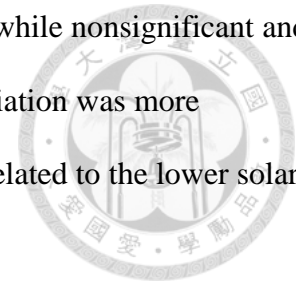
**Fig. 4.** Spatial clustering of AGC density ( $\text{kgC m}^{-2}$ ). The purple and orange shades are coldspot and hotspots of 99% significant level.

#### 3.2 Downscaled solar radiation

The downscaled daily solar radiation in MAM in the random sample (Table 1) showed



that coldspot data points had higher irradiation than other clusters, while nonsignificant and hotspot had similar amounts. However, hotspots' low incident irradiation was more elevated than coldspots and nonsignificant. This outcome may be related to the lower solar incident angle and smaller R/FR ratio.



### 3.3 Simulated wind

Based on the analysis of wind field observations from 2010-2020 (Fig. 5), we found that southwest and south directions were the prevailing wind directions during spring (March-May, MAM), summer (July-August, JJA), and winter (December-February, DJF). The median wind speeds during these seasons were 3.4, 2.2, and 4.5  $\text{ms}^{-1}$ , respectively. Additionally, we found prevailing wind directions and speeds in 2016-2020 are similar to that in 2010-2020, with spring at 216° and 3.4  $\text{ms}^{-1}$ , summer at 199° and 1.7  $\text{ms}^{-1}$ , and winter at 200° and 3.55  $\text{ms}^{-1}$ . Since we hypothesized the wind speed and direction in the growing season might link to the growth of dwarf bamboo, hence the AGC density, we simulated the spring speed and direction using WindNinja v3.8 and solved with the option of conservation of mass and momentum. However, the mesh resolution needed to be enlarged to 15 m to create a successful solution with our 5-m DSM. The statistics of the stratified sample (Table 1) showed that the mean wind speed of the three clusters was close, but the coldspot had a considerable variation. In contrast, the hotspot had a relatively steady variation. The wind directions of the three clusterings are distributed across all directions. Yet, the mean direction from coldspot to hotspot was nearly 30 degrees apart, with that of coldspot near the prevailing wind direction (216 degrees).

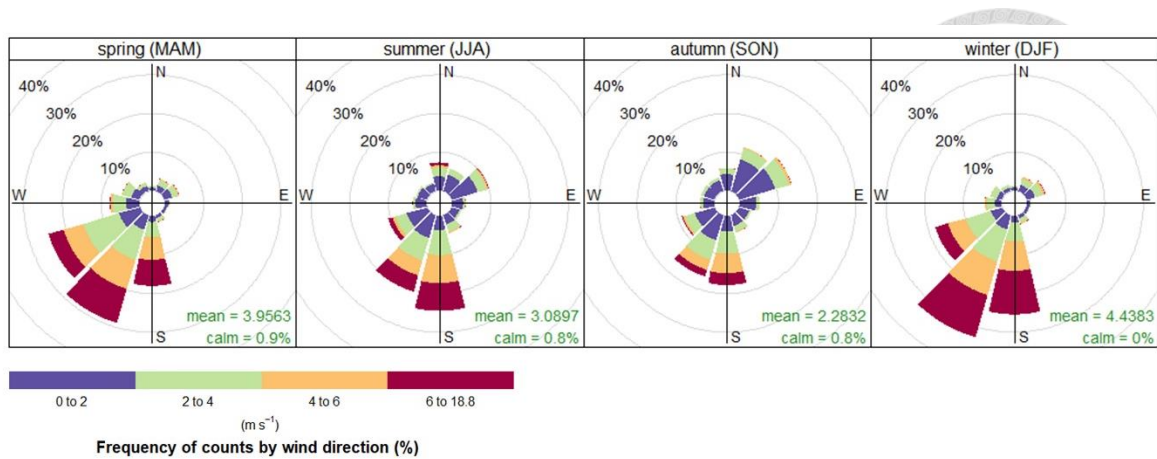


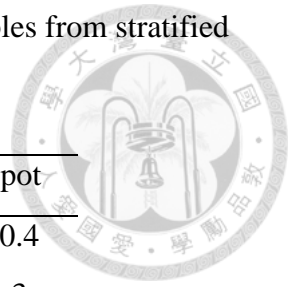
**Fig. 5.** Seasonal wind rose diagrams in 2010-2020.

### 3.4 Micro-topographical features

The micro-topographical features calculated from 1-m DEM were  $sd_{slope}$ , slope, and aspect of the focal grid. The sampled  $sd_{slope}$  of coldspot showed that the 5 x 5 m local terrain was much more homogenous than that of nonsignificant and hotspot. The slope of the coldspot was less steep, while the others were similar. The aspect of the coldspot was close to the prevailing wind direction, while the hotspot was nearly 60 degrees away from the wind direction.

**Table 1.** Summary statistics of AGC density and explanatory variables from stratified sampling (synonym refers to 2.6)

Variables	Coldspot	Nonsignificant	Hotspot
AGC	0.6±0.1	0.8±0.3	1.2±0.4
irrad	10.7±2.4	8.6±3.3	9.1±3
irrad <sub>low</sub>	0.57±0.3	0.4±0.3	0.6±0.5
speed	6.2±5	6.5±4.4	6.4±3.5
dir	207.8±79	174.8±81.9	145.5±80.1
sd <sub>slope</sub>	3.9±1.6	5.4±2.5	5.1±2.3
slope	29.7±16.6	44±18.8	41.1±16.3
aspect	198.2±95.3	178.8±94.8	146±93.3



### 3.5 Spatial clustering and environmental factors

We included the smooth function of the random sample's geographical coordinates,  $s(x,y)$ , to deal with the possible spatial autocorrelation between sample points. The Moran's  $I$  of the sample indicated that the highest value occurred at a bandwidth of 20 m (Moran's  $I = -0.31$ ,  $p = 0.001$ ), and the statistic values slowly declined to 0 ( $p = 0.46$ ) at 385 m (data not shown). Therefore, we chose a bandwidth of 20 m to check the residual conformance to the model assumption. On the other hand, the number of basis spline,  $k$ , of the coordinates smooth function was set to 100, and that of wind speed, direction, and the tensor interaction terms were 20, 50, and 10, respectively, after fine-tuning to release the residuals spatial autocorrelation in H1A. The setting was applied to the rest models for model comparison.

H1A was our benchmark to test the influence of spatial clustering of vegetation on the AGC density of dwarf bamboo and included only the abiotic factors. These were all significant, except for the main effect of wind speed. However, the interaction of wind

speed and direction had a salient partial effect, which showed that the interaction could not be ignored even though the main effect had no contribution to the model. The Moran's I reduced to 0.03 ( $p=0.06$ ) in H1A and  $s(x,y)$  might capture the spatial relationship between sample points. As a result, spring daily solar irradiation and low incident angle irradiation, wind direction, and local terrain features around the focal grid could explain the AGC density.

H1B included the spatial clustering of coldspot, nonsignificant, and hotspot, and this vegetation clustering significantly improved the model performance (Table 2). Meanwhile, residuals Moran's I dropped to 0.01 ( $p=0.31$ ). The effect of abiotic factors was reduced, and only the interaction of wind speed, direction, and slope remained significant. The apparent improvement of spatial clustering in model AIC and deviance was explained with much less degree of freedom (df). The AGC density increased with slope, and various combinations of wind speed and direction had contrasting effects on AGC density (Fig. 7).

We investigated the relationship between AGC density and environmental factors for spatial clustering with model H2. We found that the main effect of different clustering types remained significant, while environmental variables' contribution to AGC density was not significant in coldspots. This implied only the main effect of coldspot explained AGC density within the clustering. On the other hand, wind speed, interaction of wind speed and direction, and the slope linked to AGC density variation in the nonsignificant (Table 2). On the contrary, hotspot AGC density was related to spring irradiation, wind direction, the interaction of wind speed and direction,  $sd_{slope}$ , and slope.

Spring solar irradiation tended to decrease AGC density. However, AGC density increased when the wind direction was near the mean wind direction, while it decreased

when near the prevailing wind (Fig. 7). The varying combination of wind speed and direction had a contrasting influence on AGC density. The response on a slope also showed 10 and 40 degrees AGC density reach its peaks, while a slight fall in between.



**Table 2.** Model fitting results

Model	Significant covariates	Deviance Explained	AIC	df
H1A	s(x,y) <sup>***</sup> , s(irrad) <sup>**</sup> , s(irrad <sub>low</sub> ) <sup>*</sup> , s(dir) <sup>*</sup> , ti(speed,dir) <sup>***</sup> s(slope) <sup>*</sup> , s(aspect) <sup>***</sup>	39.2%	990	94
H1B	s(x,y) <sup>**</sup> , Coldspot <sup>***</sup> , Nonsig <sup>***</sup> , Hotspot <sup>***</sup> , ti(speed,dir) <sup>*</sup> , s(slope) <sup>*</sup>	49.1%	641	52
H2	Coldspot <sup>***</sup> , Nonsig <sup>***</sup> , Hotspot <sup>***</sup> , s(irrad):Hotspot <sup>*</sup> , s(speed):Nonsig <sup>*</sup> , s(dir):Hotspot <sup>***</sup> , ti(speed,dir):Nonsig <sup>*</sup> , ti(speed,dir):Hotspot <sup>***</sup> , s(sd <sub>slope</sub> ):Hotspot <sup>**</sup> , s(slope):Nonsig <sup>*</sup> , s(slope):Hotspot <sup>*</sup>	53.2%	574	83

s(x): cluster is interaction between specific cluster and smooth function of x

<sup>\*\*\*</sup>  $p < 0.001$ ; <sup>\*\*</sup>  $p < 0.01$ ; <sup>\*</sup>  $p < 0.05$

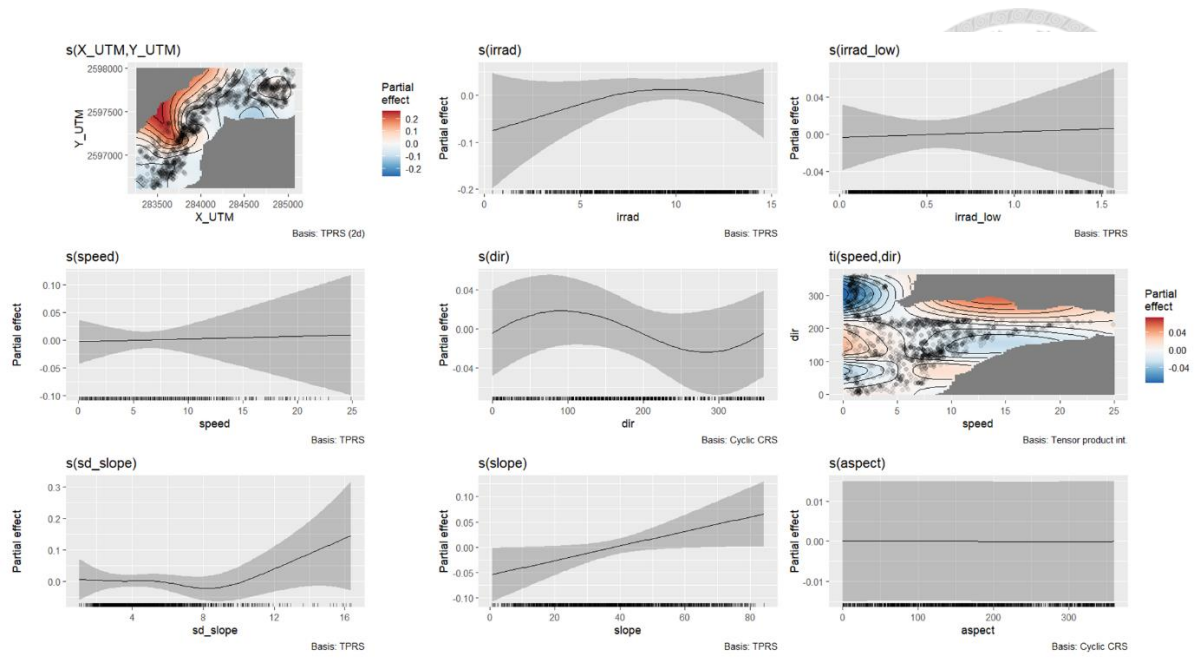


**Fig. 6.** Effect of spatial cluster types and environment factors on AGC density

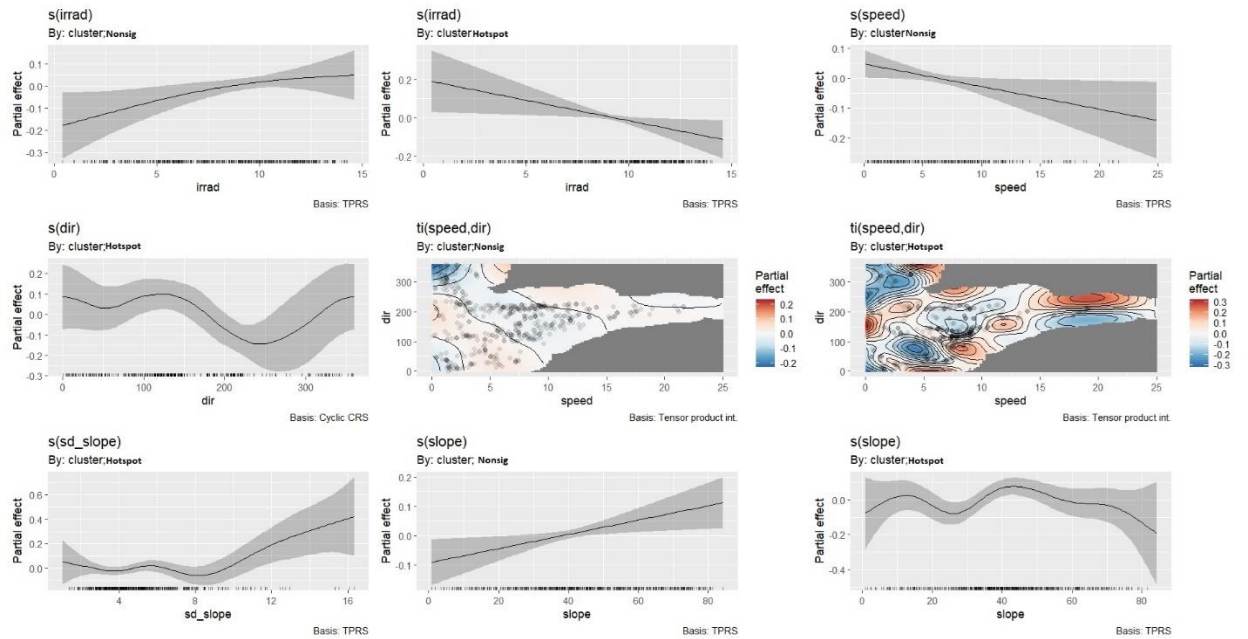


**Fig. 7.** Effect of spatial cluster types and environment factors interactions on AGC density

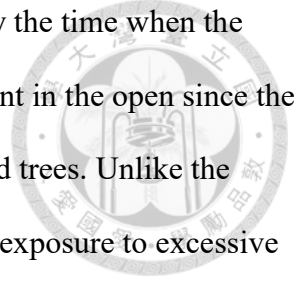
## 4. Discussions

### 4.1 Environmental factors and spatial clustering

Mean annual precipitation and temperature depict the distribution of different biomes

(Whittaker, 1975), and hence the main plant communities' aboveground biomass and carbon storage density. However, the small vegetation habitats comprising contrasting environmental gradients shaped by the complex mountainous terrain in an altitudinal belt may require local data to describe the AGC density variation. Solar irradiance, prevailing wind patterns in the growing season, and micro-topographic features were assessed for the influence on and relationship with AGC density of dwarf bamboo vegetation. Additionally, we introduced the spatial clustering of AGC density as the biotic variable to assess the AGC density variation amount.

We found that spatial clustering substantially influences the relationship between environmental factors and AGC density (Table 2). While it is commonly assumed that factors like solar radiation, wind speed, and micro-topography affect plant growth, aboveground biomass, and AGC density, this study found that incorporating spatial clustering into models significantly improved model performance. It shrunk the contribution of most environmental variables, leaving the interaction of wind speed and direction, and slope remained significant. Springtime wind speed and direction interaction were substantial in both models with or without spatial clustering of the vegetation, suggesting the role of wind pattern contributed to AGC density in subalpine areas. Even though springtime daily solar irradiation and low incident angle may affect the temperature and heat accumulated under contrasting settings of topography and neighbors (Fig. 1), as shown in the result of model H1A, the presence of spatial clustering of AGC density shrunk the effect of irradiation. The AGC density was estimated with lidar point cloud height percentile of 95th, 65th, and maximum and positively related to the top and 65th percentile; hence, high AGC density implies a large body size in situ. Therefore, coldspots and hotspots indicated the focal grids were surrounded by dwarf bamboo of similar body size.

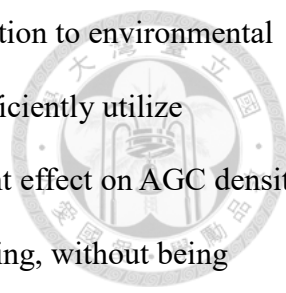


Measurements and inferences of AGC density were carried out by the time when the dwarf bamboo stayed in a dynamic equilibrium and became dominant in the open since the wildfire torched in 1993, which nearly burned off dwarf bamboo and trees. Unlike the vegetation recovers from disturbance or newly colonized where the exposure to excessive solar radiation and wind may negatively impact the survival and growth of vegetation, establishing coldspot or hotspot clustering implies the vegetation has acclimated to the local environmental factors and formed its microclimate around and beneath the canopy, suggesting that the impact of environmental factors on AGC density in the vegetation may be less than the effect of vegetation spatial clustering. Although the slope standard deviation measures the surface roughness in the neighborhood and may be used as proxies for unmeasured variables of surface drainage and soil moisture, the non-significance may possibly be related to the microclimate created by vegetation clustering near the surface.

#### 4.2 Spatial clustering leads to differing responses to environmental factors

Vegetations like forests can create a microclimate beneath their canopies and buffer or mitigate the impact from the macro-climate and also influence the local climate (Frenne et al., 2021), and closed canopy forests make the microclimate beneath relatively stable and slow understory community composition shifts, while open canopy forests tend to accelerate the shift due to warming macro-climate (Zellweger et al., 2020). The spatial clustering may facilitate dwarf bamboo vegetation to moderate the impact of the environment and response to environmental gradients. The influence of environmental factors on AGC density under spatial clustering (Table 2) indicates the presence of an interaction between environmental factors and spatial clustering types. Since spatial clustering, especially hotspots, results from acclimation to the environment, it could be viewed as the indirect effect of the environment as biomass accumulation (Michaletz et al., 2014) and growth history.





Dwarf bamboo in the hotspot was large in body size, and acclimation to environmental gradients may mitigate the impact of unfavorable conditions and efficiently utilize resources. On the contrary, environmental factors have no significant effect on AGC density in the coldspot, meaning AGC density is only affected by its clustering, without being affected by springtime daily solar radiation or low incident angle radiation and wind pattern. Since the dwarf bamboo demonstrates contrasting changes in leaf morphological and physiological traits under different light conditions (Wu & Kao, 2021), dwarf bamboo in the coldspot with high solar irradiation (Table 1) may alter the morphological and physiological traits to fit the environment, making the environment much less critical to AGC density. Since the height percentiles of UAV-lidar returns estimate the high or low values of AGC density, we argue that the canopy structure is linked directly to spatial clustering and altered phenotypic traits. The spatial clustering types condition the various responses of AGC density on environmental gradients. The competition or facilitation between dwarf bamboo and neighboring trees was not assessed because these interactions happen in the interface or forest edge and are mainly located in the hotspot, these effects of interactions may have been mixed with irradiation and wind pattern.

Abiotic factors such as precipitation and soil physical and chemical properties may also link to AGC density. However, including or upscaling the measurement of these properties are beyond the scope of this study. Our study area has an average annual rainfall of 2838 mm. It is humid throughout the year (Fig. 2). Also, spatial data such as soil thickness or texture were unavailable. Hence, it was impossible to evaluate soil's direct influence on AGC density in our analysis.

Furthermore, since bamboo is a fast-growing species and its growth season is mainly in spring, this study focused only on the effect of spring radiation. It did not consider the

possible accumulation effects of radiation in other seasons. On the other hand, herbivory was also not included in this study as a control variable; therefore, its influences were not assessed. However, from the perspective of the hypothesis proposed, locations without high- or low-value clusters are more salient than environmental factors. Sites of hotspots exhibit diverse adaptive conditions, and such vegetation clusters almost exclusively influence those in coldspots. Traditional studies may overestimate the contribution of environmental factors' contribution to AGC density without considering spatial clustering types, especially when dwarf bamboo cover is dominant. Hence spatially explicit estimation of AGC density solely based on environmental factors may have limited capacity to predict on a finer scale.

## **5. Conclusion**

We utilized downscaled spring hourly solar radiation data, prevailing wind field simulation, micro topographical features, and finer-scale AGC density to understand the effects of vegetation clustering types and environmental factors on AGC density. We proposed two hypotheses: H1 - that vegetation spatial clustering explains more variance in AGC density than environmental factors, and H2 - vegetation spatial clustering moderates AGC density response on environmental gradients. We used stratified random sampling for spatial clustering of coldspot, nonsignificant, with 500 grids for each stratum and GAM models to assess our hypotheses. Our results showed that vegetation clustering types had a more significant influence on AGC density than other environmental factors and different spatial clustering types had different adaptive mechanisms for environmental factors. This

indicates that the impact of spatial clustering should not be ignored when evaluating or estimating AGC density using environmental factors.



### **Acknowledgments**

We appreciate the field assistance provided by Wen-Tiao Liao and Ciou-Hui Wu. This work was supported by the National Science and Technology Council (111-2121-M-002-001-), Taiwan Forestry Research Institute (111AS-7.1.2-FI-G1), National Taiwan University (NTU-107L9010) and the Research Center for Future Earth, the Featured Areas Research Center Program, the Higher Education Sprout Project, and the Ministry of Education (MOE) in Taiwan.

### **Declaration of interest statement**

The corresponding author confirms on behalf of all authors that there have been no involvements that might raise the question of bias in the work reported or in the conclusions, implications, or opinions stated.

### **Author contributions statement**

Hsiao-Lung Pan: Formal analysis, Data curation, Resources, Conceptualization, Methodology, Investigation, Resources, Data curation, Writing - original draft, Visualization, Project administration, Funding acquisition

Cho-ying Huang: Conceptualization, Methodology, Investigation, Resources, Data curation, Writing - original draft, Writing - review & editing, Visualization, Supervision, Funding acquisition

### **Data availability statement**


The data that support the findings of this study will be openly available in Zenodo upon the acceptance of the manuscript.





## References

- Baskin, J. M. (2009). Death of bamboo triggers regeneration of overstory tree in a southern beech forest. *New Phytologist*, *181*(4), 749–750. <https://doi.org/10.1111/j.1469-8137.2009.02757.x>
- Bickford, C., Hunt, J., & Heenan, P. (2011). Microclimate characteristics of Southern Alps bluff ecosystems and implications for plant growth. *New Zealand Journal of Ecology*, *35*, 273–279.
- Carslaw, D. C., & Ropkins, K. (2012). openair—An R package for air quality data analysis. *Environmental Modelling & Software*, *27–28*, 52–61. <https://doi.org/10.1016/j.envsoft.2011.09.008>
- Forthofer, J., Butler, B., & Wagenbrenner, N. (2014). A comparison of three approaches for simulating fine-scale surface winds in support of wildland fire management. Part I. Model formulation and comparison against measurements. *International Journal of Wildland Fire*, *23*. <https://doi.org/10.1071/WF12089>
- Frenne, P., Lenoir, J., Luoto, M., Scheffers, B., Zellweger, F., Aalto, J., Ashcroft, M., Christiansen, D., Decocq, G., De Pauw, K., Govaert, S., Greiser, C., Gril, E., Hampe, A., Jucker, T., Klinges, D., Koelemeijer, I., Lembrechts, J., Marrec, R., & Hylander, K. (2021). Forest microclimates and climate change: Importance, drivers and future research agenda. *Global Change Biology*, *27*. <https://doi.org/10.1111/gcb.15569>
- James, G., Witten, D., Hastie, T., & Tibshirani, R. (2021). *An Introduction to Statistical Learning: With Applications in R (Hardcover)* (Second). Springer. <https://www.statlearning.com/>
- Lindsay, J. (2014). *The Whitebox Geospatial Analysis Tools project and open-access GIS*.
- Maclean, I. M. D., Mosedale, J. R., & Bennie, J. J. (2019). Microclima: An r package for modelling meso- and microclimate. *Methods in Ecology and Evolution*, *10*(2), 280–290. <https://doi.org/10.1111/2041-210X.13093>
- Marquis, B., Bergeron, Y., Simard, M., & Tremblay, F. (2021). Disentangling the effect of topography and microtopography on near-ground growing-season frosts at the boreal-temperate forest ecotone (Québec, Canada). *New Forests*, *52*(6), 1079–1098. <https://doi.org/10.1007/s11056-021-09840-7>

- 
- Michaletz, S. T., Cheng, D., Kerkhoff, A. J., & Enquist, B. J. (2014). Convergence of terrestrial plant production across global climate gradients. *Nature*, *512*(7512), Article 7512. <https://doi.org/10.1038/nature13470>
- Missoula Fire Sciences Laboratory. (n.d.). *WindNinja Tutorials*. Retrieved May 3, 2023, from <https://weather.firelab.org/windninja/tutorials/>
- National Renewable Energy Laboratory. (n.d.). *NSRDB*. Retrieved July 7, 2023, from <https://nsrdb.nrel.gov/>
- Panigrahy, M., Majeed, N., & Panigrahi, K. C. S. (2020). Low-light and its effects on crop yield: Genetic and genomic implications. *Journal of Biosciences*, *45*(1), 102. <https://doi.org/10.1007/s12038-020-00070-1>
- Privé, J.-P., & Allain, N. (2000). Wind reduces growth and yield but not net leaf photosynthesis of primocane-fruited red raspberries (*Rubus idaeus* L.) in the establishment years. *Canadian Journal of Plant Science*, *80*(4), 841–847. <https://doi.org/10.4141/P99-170>
- Schindler, D., Bauhus, J., & Mayer, H. (2012). Wind effects on trees. *European Journal of Forest Research*, *131*(1), 159–163. <https://doi.org/10.1007/s10342-011-0582-5>
- Wagenbrenner, N. S., Forthofer, J. M., Lamb, B. K., Shannon, K. S., & Butler, B. W. (2016). Downscaling surface wind predictions from numerical weather prediction models in complex terrain with WindNinja. *Atmospheric Chemistry and Physics*, *16*(8), 5229–5241. <https://doi.org/10.5194/acp-16-5229-2016>
- Whittaker, R. H. (1975). *Communities and ecosystems*.
- Wood, S. N. (2017). *Generalized Additive Models: An Introduction with R, Second Edition* (2nd ed.). Chapman and Hall/CRC. <https://doi.org/10.1201/9781315370279>
- Wu, K.-S., & Kao, W.-Y. (2021). Phenotypic plasticity and genetic variation in leaf traits of *Yushania niitakayamensis* (Bambusoideae; Poaceae) in contrasting light environments. *Journal of Plant Research*. <https://doi.org/10.1007/s10265-021-01327-y>
- Zellweger, F., De Frenne, P., Lenoir, J., Vangansbeke, P., Verheyen, K., Bernhardt-Römermann, M., Baeten, L., Hédli, R., Berki, I., Brunet, J., Van Calster, H., Chudomelová, M., Decocq, G., Dirnböck, T., Durak, T., Heinken, T., Jaroszewicz, B., Kopecký, M., Máliš, F., ... Coomes, D. (2020). Forest microclimate dynamics drive plant responses to warming. *Science*, *368*(6492), 772–775.

<https://doi.org/10.1126/science.aba6880>

